

การติดตามการเกิดซีส-ทรานส์โฟโตไอโซเมอไรเซชันของออกทิลเมธอกซีซินนามัต
ด้วยเทคนิคเอทีอาร์-เอฟทีไออาร์สเปกโทรสโกปี



นางสาวภัทราภรณ์ แผงนคร

สถาบันวิทยบริการ จุฬาลงกรณ์มหาวิทยาลัย

วิทยานิพนธ์นี้เป็นส่วนหนึ่งของการศึกษาตามหลักสูตรปริญญาวิทยาศาสตรมหาบัณฑิต

สาขาวิชาเคมี ภาควิชาเคมี

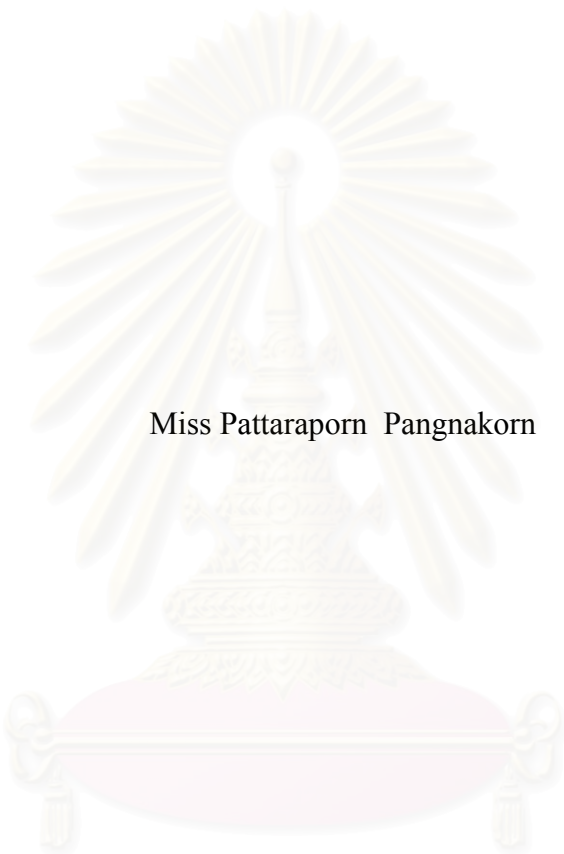
คณะวิทยาศาสตร์ จุฬาลงกรณ์มหาวิทยาลัย

ปีการศึกษา 2547

ISBN 974-53-1488-9

ลิขสิทธิ์ของจุฬาลงกรณ์มหาวิทยาลัย

INVESTIGATION OF *CIS-TRANS* PHOTOISOMERIZATION
OF OCTYL METHOXYCINNAMATE BY ATR-FTIR SPECTROSCOPY



Miss Pattaraporn Pagnakorn

สถาบันวิทยบริการ
จุฬาลงกรณ์มหาวิทยาลัย

A Thesis Submitted in Partial Fulfillment of the Requirements

for the Degree of Master of Science in Chemistry

Department of Chemistry

Faculty of Science

Chulalongkorn University

Academic Year 2004

ISBN 974-53-1488-9

Thesis Title INVESTIGATION OF *CIS-TRANS* PHOTOISOMERIZATION
 OF OCTYL METHOXYCINNAMATE BY ATR-FTIR
 SPECTROSCOPY

By Miss Pattaraporn Pangnakorn

Field of Study Chemistry

Thesis Advisor Associate Professor Supason Wanichweacharunguang, Ph.D.

Thesis Co-Advisor Assistant Professor Sanong Ekgasit, Ph.D.

Accepted by the Faculty of Science, Chulalongkorn University in Partial
Fulfillment of the Requirements for the Master's Degree

.....Dean of the Faculty of Science
(Professor Piamsak Menasveta, Ph.D.)

THESIS COMMITTEE

..... Chairman
(Professor Udom Kokpol, Ph.D.)

..... Thesis Advisor
(Associate Professor Supason Wanichweacharunguang, Ph.D.)

..... Thesis Co-Advisor
(Assistant Professor Sanong Ekgasit, Ph.D.)

..... Member
(Associate Professor Chuchaat Thammacharoen)

..... Member
(Assistant Professor Vipavee P.Hoven, Ph.D.)

ภัทรภรณ์ แผงนคร: การติดตามการเกิดซิส-ทรานส์โฟโตไอโซเมอไรเซชันของออกทิลเมธอกซีซินนาเมต ด้วยเทคนิคเอทีอาร์-เอฟทีไออาร์สเปกโทรสโกปี (INVESTIGATION OF CIS-TRANS PHOTOISOMERIZATION OF OCTYL METHOXYCINNAMATE BY ATR-FTIR SPECTROSCOPY), อาจารย์ที่ปรึกษา: รศ.ดร.ศุภศร วณิชเวชารุ่งเรือง และ ผศ.ดร.สนอง เอกสิทธิ์ 63 หน้า. ISBN 974-53-1488-9

งานวิจัยนี้ได้ทำการติดตามการเกิดโฟโตไอโซเมอไรเซชันของสารกรองรังสียูวีบี ออกทิลเมธอกซีซินนาเมต (OMC) บนพื้นผิว ด้วยเทคนิคแอทเทนนูเอตเททโททอลรีเฟรคชันฟูเรียร์ทรานสฟอร์ม อินฟราเรด หรือ เอทีอาร์-เอฟทีไออาร์สเปกโทรสโกปี (ATR-FTIR) จากการศึกษาพบว่า สมดุลโฟโตสแตชันนารีของการเปลี่ยนคอนฟิเจอร์ชันจาก *E*-OMC ไปเป็น *Z*-OMC และจาก *Z*-OMC ไปเป็น *E*-OMC ขึ้นกับปริมาณของ OMC บนพื้นผิว โดยพบว่า การเปลี่ยนคอนฟิเจอร์ชันจะเกิดมากขึ้นเมื่อปริมาณของ OMC ลดลง โดยในงานวิจัยนี้ได้ติดตามการเปลี่ยนคอนฟิเจอร์ชันของ OMC บนพื้นผิวซิงค์ซัลไฟด์และผิวของลูกหนูหริ่ง (*Mus musculus* Linn.) โดยพบการเปลี่ยนคอนฟิเจอร์ชันทั้งจาก *E* ไปเป็น *Z* และ จาก *Z* ไปเป็น *E* บนพื้นผิวหนังหนู มากกว่าบนพื้นผิวซิงค์ซัลไฟด์เล็กน้อย ที่ปริมาณการกระจายของ OMC บนผิวหนังประมาณ 2 มิลลิกรัมต่อตารางเซนติเมตร หรือ 6.89×10^{-6} โมลต่อตารางเซนติเมตร ซึ่งเป็นปริมาณการกระจายของสารกรองรังสียูวีบีที่แนะนำให้ใช้บนผิวหนัง ยังคงพบการเปลี่ยนคอนฟิเจอร์ชันที่ความเข้มของรังสียูวีบี 0.08 มิลลิวัตต์ต่อตารางเซนติเมตร (เป็นความเข้มของรังสียูวีบีที่ใกล้เคียงกับที่วัดได้ในแสงแดดช่วงใกล้เที่ยงในประเทศไทย ในวันที่ท้องฟ้าปลอดโปร่ง) โดยจากการทดลองบนหนังหนูที่สภาวะดังกล่าวพบว่า ที่สมดุลโฟโตสแตชันนารี มีสัดส่วนของ *E*-OMC ต่อ *Z*-OMC ประมาณ 3:1

สถาบันวิทยบริการ
จุฬาลงกรณ์มหาวิทยาลัย

ภาควิชา.....เคมี.....ลายมือชื่อนิสิต.....
สาขาวิชา.....เคมี.....ลายมือชื่ออาจารย์ที่ปรึกษา.....
ปีการศึกษา.....2547.....ลายมือชื่ออาจารย์ที่ปรึกษาร่วม.....

4572434123 : MAJOR CHEMISTRY

KEY WORD : OCTYL METHOXYCINNAMATE/ PHOTOISOMERIZATION/
SUNSCREEN/ ATR-FTIR SPECTROSCOPY

PATTARAPORN PANGNAKORN: INVESTIGATION OF *CIS-TRANS* PHOTOISOMERIZATION OF OCTYL METHOXYCINNAMATE BY ATR-FTIR SPECTROSCOPY. THESIS ADVISOR: ASSOC. PROF. SUPASON WANICHWEACHARUNGRUANG, Ph.D., ASST. PROF. SANONG EKGASIT, Ph.D. 63 pp. ISBN 974-53-1488-9

In this work, photoisomerization of the UVB filter octyl methoxycinnamate (OMC) on surface was monitored using ATR-FTIR spectroscopy. The study showed that photostationary equilibrium of both the *E*- to *Z*-OMC and the *Z*- to *E*-OMC was affected by amount of OMC coverage on the surface. More configurational changes were found at lower coverage of OMC. In this work, the configurational change was monitored on ZnSe and rat skin (*Mus musculus* Linn.) surface. A little more configurational changes were detected on rat skin comparing to on ZnSe surface. At the OMC coverage of 2 mg/cm² or 6.89×10⁻⁶ moles/cm² which represents the on skin recommended use of OMC, *E* to *Z* configurational change was detected at the UVB irradiance of 0.08 mW/cm² (correspond to UVB irradiance detected in sunlight in Bangkok at noon time on clear sky day). At such condition, photostationary equilibrium of the *E*- to *Z*-OMC on rat skin gave the *E*-OMC: *Z*-OMC ratio of about 3:1

สถาบันวิทยบริการ
จุฬาลงกรณ์มหาวิทยาลัย

Department.....Chemistry.....Student's signature.....

Field of Study.....Chemistry.....Advisor's signature.....

Academic year.....2004.....Co-advisor's signature.....

ACKNOWLEDGEMENTS

I would like to express my appreciation to my advisor, Associate Professor Dr. Supason Wanichweacharungruang for all her substantial advices, precious assistance and encouragement on my research. Sincere thanks are also extended to Assistant Professor Dr. Sanong Ekgasit, my co-advisor, who always provides me the valuable suggestion.

I greatly appreciated the Faculty of Science and Graduated School, Chulalongkorn University for the partial financial support on this research work. I also gratefully thank Department of Chemistry, Chulalongkorn University.

Special thanks are extended to all members in Dr. Supason's group for their discussions, opinions, and encouragement. I also thank all members in the Sensor Research Unit, Department of Chemistry, Chulalongkorn University.

Finally, I would like to affectionately give all my gratitude to my mother and the members of my family for their love, encouragement, understanding and consistently patience throughout my entire study. Without them, I would never have been able to achieve this goal.



สถาบันวิทยบริการ
จุฬาลงกรณ์มหาวิทยาลัย

CONTENTS

	Page
ABSTRACT IN THAI	iv
ABSTRACT IN ENGLISH	v
ACKNOWLEDGEMENTS	vi
LIST OF FIGURES	ix
LIST OF TABLE	xiii
LIST OF ABBREVIATIONS	xiv
LIST OF SYMBOLS	xiv
LIST OF UNITS	xiv
CHAPTER I INTRODUCTION	1
1.1 Ultraviolet (UV) radiation	1
1.1.1 Health effects	1
1.1.2 Protection	3
1.2 Sunscreen Chemicals	3
1.2.1 Classification of Sunscreen Chemicals	3
1.2.2 Sunscreen Chemical Characters	5
1.3 Mechanism of Organic UV Filters	5
1.4 Octyl Methoxycinnamate (OMC)	7
1.5 Attenuated Total Reflectance Fourier Transform Infrared (ATR-FTIR) Spectroscopy	9
1.5.1 Information provided from ATR-FTIR spectroscopy	9
1.5.2 Principle of the ATR Technique	9
1.5.3 ATR crystal materials and accessories	11
1.5.4 Analyzing liquids	12
1.6 Objectives	13
CHAPTER II EXPERIMENTAL	14
2.1 Materials	14
2.2 Chemicals	15

2.3 Preparation of OMC solutions	15
2.3.1 Preparation of <i>E</i> -OMC solutions	15
2.3.2 Preparation of <i>Z</i> -OMC	16
2.3.3 Preparation of <i>E</i> -OMC and <i>Z</i> -OMC for calibration standard and for <i>Z</i> to <i>E</i> photoisomerization	16
2.4 Nuclear magnetic resonance (NMR) spectroscopy.....	17
2.5 Attenuated Total Reflection Fourier Transform Infrared (ATR-FTIR) Spectroscopy	17
2.5.1 Single Reflection System.....	18
2.5.2 Multiple Reflection System	19
2.5.2.1 Kinetic study of <i>E</i> to <i>Z</i> Photoisomerization on ZnSe	19
2.5.2.2 Kinetic study of <i>E</i> to <i>Z</i> photoisomerization on rat skin.....	20
2.5.2.3 Kinetic study of <i>Z</i> to <i>E</i> photoisomerization on ZnSe....	21
2.5.2.4 Binary-phase calibration standards	21
2.6 Data analysis	22
CHAPTER III RESULTS AND DISCUSSION.....	23
3.1 Purification of <i>Z</i> -OMC.....	23
3.2 Binary-phase calibration standards	30
3.3 Kinetic study of <i>E</i> to <i>Z</i> Photoisomerization on ZnSe	32
3.4 Kinetic study of <i>E</i> to <i>Z</i> Photoisomerization on rat skin.....	40
3.5 Kinetic study of <i>Z</i> to <i>E</i> Photoisomerization on ZnSe	44
CHAPTER IV CONCLUSION	49
REFERENCES	50
APPENDICES	53
APPENDIX A	54
APPENDIX B	57
VITA.....	63

LIST OF FIGURES

Figure	Page
1.1 Electromagnetic spectrum.....	2
1.2 Depth of UV penetration into the skin.....	2
1.3 Structures of the commonly used UV filters.....	4
1.4 Mechanism of sunscreen action.....	6
1.5 Structure of Octyl methoxycinnamate (OMC)	7
1.6 Conversion of <i>E</i> -OMC to <i>Z</i> -OMC after exposure to UV radiation	8
1.7 The common IRE configurations: (A) single-reflection variable angle hemispherical crystal and (B) multiple-reflection planar crystal.....	10
1.8 Total internal reflection at the interface of an internal reflection element .	10
1.9 ZnSe crystal	12
2.1 Radiation from the UVB lamp used in the experiment.....	14
2.2 The Seagull™ Variable Angle Reflection Attachment.....	18
2.3 The layout of the irradiation unit	20
2.4 Instrumental setup for kinetic studies on rat specimens	21
3.1 ¹ H-NMR of a mixture of <i>E</i> - and <i>Z</i> -OMC (light exposed OMC solution) (A), standard <i>E</i> -OMC (B), isolated <i>Z</i> -OMC (C).....	22
3.2 Spectrum of <i>trans</i> -OMC (<i>E</i> -OMC) in the frequency range of 600-3200 cm ⁻¹	25
3.3 Spectrum of <i>cis</i> -OMC (<i>Z</i> -OMC) in the frequency range of 600-3200 cm ⁻¹	25
3.4 ATR-FTIR spectrum of <i>E</i> -OMC (A) and <i>Z</i> -OMC (B)	26
3.5 Expansion of the ATR-FTIR spectra of the <i>E</i> - and the <i>Z</i> -OMC in the 1665-1610 cm ⁻¹ range	28
3.6 The differences of spectral intensities between the <i>E</i> - and <i>Z</i> -isomer in the frequency range of 720-680 cm ⁻¹	28
3.7 The differences of spectral intensities between the <i>E</i> - and <i>Z</i> -isomer in the frequency range of 998-964 cm ⁻¹	29
3.8 Overlaid ATR-FT-IR transmittance spectra of <i>E</i> - <i>Z</i> mixtures containing 0, 10, 25, 50, 75, 90, and 100 mole percent of <i>Z</i> -isomer in the mixtures of <i>E</i> - and <i>Z</i> -OMC	30

- 3.9 Calibration plot between **b/a** and mole percent of Z-OMC from ATR-FTIR taken of the binary -phase mixtures31
- 3.10 ATR-FTIR spectra showing photoisomerization of *E*-OMC on ZnSe at various times of exposure. Coverages of OMC on ZnSe were 3.44×10^{-7} moles/cm² (A), 6.89×10^{-7} moles/cm² (B), 1.38×10^{-6} moles/cm² (C) and 2.04×10^{-6} moles/cm² (D), respectively.....32
- 3.11 ATR-FTIR spectra showing photoisomerization of *E*-OMC on ZnSe at various times of exposure. These spectra are the expansions of the spectra in Figure 3.10.....33
- 3.12 Plot of the peak area ratios **b/a** as a function of UVB exposure time from the *E* to *Z* experiment on ZnSe for (■) 3.44×10^{-7} moles/cm²; (◆) 6.89×10^{-7} moles/cm²; (▲) 1.38×10^{-6} moles/cm²; (●) 2.04×10^{-6} moles/cm² OMC coverage34
- 3.13 Plot of the mole percent of the Z-OMC as a function of UVB exposure time from the *E* to *Z* experiment on ZnSe for (■) 3.44×10^{-7} moles/cm²; (◆) 6.89×10^{-7} moles/cm²; (▲) 1.38×10^{-6} moles/cm²; (●) 2.04×10^{-6} moles/cm² OMC coverage.35
- 3.14 ATR-FTIR spectra showing photoisomerization of *E*-OMC on ZnSe at various times of exposure. Coverages of OMC on ZnSe were 3.44×10^{-6} moles/cm² (A), 6.89×10^{-6} moles/cm² (B) and 1.38×10^{-5} moles/cm² (C), respectively.....36
- 3.15 ATR-FTIR spectra showing photoisomerization of *E*-OMC on ZnSe at various times of exposure. These spectra are the expansions of the spectra in Figure 3.14.....37
- 3.16 Plot of the peak area ratios **b/a** as a function of UVB exposure time from the *E* to *Z* experiment for (◆) 3.44×10^{-6} moles/cm²; (▲) 6.89×10^{-6} moles/cm²; (■) 1.38×10^{-5} moles/cm² of OMC on ZnSe.....38
- 3.17 Plot of the mole percent of the Z-OMC as a function of UVB exposure time from the *E* to *Z* experiment for (◆) 3.44×10^{-6} moles/cm²; (▲) 6.89×10^{-6} moles/cm²; (■) 1.38×10^{-5} moles/cm² of OMC on ZnSe.....38

Figure	Page
3.18	Plot of UVB intensities in Bangkok measured during the day39
3.19	ATR-FTIR spectra showing photoisomerization of <i>E</i> -OMC on rat skin at various times of exposure. Coverages of OMC on ZnSe were 3.44×10^{-6} moles/cm ² (A), 6.89×10^{-6} moles/cm ² (B) and 1.38×10^{-5} moles/cm ² (C), respectively.....40
3.20	ATR-FTIR spectra showing photoisomerization of <i>E</i> -OMC on rat skin at various times of exposure. These spectra are the expansions of the spectra in Figure 3.19.....41
3.21	Plot of the peak area ratios b/a as a function of UVB exposure time from the <i>E</i> to <i>Z</i> experiment for (▲) 3.44×10^{-6} moles/cm ² ; (◆) 6.89×10^{-6} moles/cm ² ; (■) 1.38×10^{-5} moles/cm ² of OMC on rat skin.42
3.22	Plot of the mole percent of the <i>Z</i> -OMC as a function of UVB exposure time from the <i>E</i> to <i>Z</i> experiment for (▲) 3.44×10^{-6} moles/cm ² ; (◆) 6.89×10^{-6} moles/cm ² ; (■) 1.38×10^{-5} moles/cm ² of OMC on rat skin .42
3.23	Plot of the mole percent of the <i>Z</i> -OMC as a function of UVB exposure time from the <i>E</i> to <i>Z</i> experiment for (■) 3.44×10^{-7} moles/cm ² ; (◆) 6.89×10^{-7} moles/cm ² ; (▲) 1.38×10^{-6} moles/cm ² ; (●) 2.04×10^{-6} moles/cm ² ; (◆) 3.44×10^{-6} moles/cm ² ; (▲) 6.89×10^{-6} moles/cm ² and (■) 1.38×10^{-5} moles/cm ² of OMC on ZnSe.....43
3.24	ATR-FTIR spectra showing photoisomerization of <i>Z</i> -OMC on ZnSe at various times of exposure. Coverage of OMC on ZnSe was 1.34×10^{-7} moles/cm ²44
3.25	Expansion of the ATR-FTIR spectra in the 1100-900 cm ⁻¹ range showing photoisomerization of <i>Z</i> -OMC on ZnSe after various UVB exposure times (between 0-60 min).....45
3.26	Plot of the peak area ratios b/a as a function of UVB exposure times for 1.34×10^{-7} moles/cm ² of OMC on ZnSe. (A) <i>Z</i> - to <i>E</i> -photoisomerization: (B) <i>E</i> - to <i>Z</i> -photoisomerization.....46
3.27	Plot of the mole percent of the <i>Z</i> -OMC as a function of UVB exposure time for (A) <i>Z</i> to <i>E</i> photoisomerization, (B) <i>E</i> to <i>Z</i> photoisomerization.....47

LIST OF TABLE

Tables	Page
1.2 ATR Crystal Properties.	11
2.1 Concentration of prepared OMC solution.....	14
2.2 Shows volumes of 0.0033 M <i>E</i> -OMC and 0.0033 M <i>Z</i> -OMC used in preparing calibration standards.....	16
2.3 Dispersion of OMC on ZnSe's surface area 5.0×0.5 cm ²	18
3.1 Vibrational spectral assignments of OMC in the Infrared.....	26



สถาบันวิทยบริการ
จุฬาลงกรณ์มหาวิทยาลัย

LIST OF ABBREVIATIONS

ATR	attenuated total reflection	NMR	nuclear magnetic resonance
CDCl ₃	deuterated chloroform	M.W.	molecular weight
d	doublet	s	singlet (NMR)
FT-IR	Fourier transform infrared	UV	ultraviolet
IR	infrared	UVA	ultraviolet A
IRE	internal reflection element	UVB	ultraviolet B
OMC	octyl methoxycinnamate	UVC	ultraviolet C
<i>J</i>	Coupling constant	ZnSe	zinc selenide

LIST OF SYMBOLS

%	percent
λ	wavelength
θ	theta
δ	chemical shift
ϵ	molar absorptivity

LIST OF UNITS

°C	degree Celsius
cm ⁻¹	per centimeter (s)
g	gram (s)
Hz	hertz
mL	milliliter (s)
nm	nanometer (s)
mol	mole

CHAPTER I

INTRODUCTION

1.1 Ultraviolet (UV) radiation

Energy from the sun comes to the earth in the form of electromagnetic radiation. The sun radiates energy in a wide range of wavelengths, most of which are invisible to human eyes. Ultraviolet (UV) radiation that reaches the earth's surface is in wavelengths between 290 and 400 nm. This is shorter than wavelengths of visible light, which are 400 to 700 nm. Ultraviolet radiation can be divided into the following regions: UVA (320–400 nm), UVB (280–320 nm) and UVC (200–280 nm) (Figure 1.1). Although UVC is the most harmful UV radiation, it is filtered out by the ozone layer before reaching the earth's surface. The UVB radiation, which is partially filtered by ozone, can penetrate both the stratum corneum and the epidermis of human skin (1) (Figure 1.2). It has sufficient energy to cause damage, such as sunburn, to human skin. This is particularly true for fair-skinned individuals. The radiation in the UVA region, which is unfiltered by ozone, has deeper penetration human skin to the dermis; it, thereby, stimulates the formation of melanin and produces a tan, which acts as the first line of defense for the protection from sunburn. UVA radiation, therefore, is also called the “tanning region.” Although having considerably lower energy than UVB, UVA photons can cause delayed damages to the skin. (2)

1.1.1 Health effects

UVB light has been related to skin cancers (3) such as melanoma. The radiation ionizes DNA molecules in skin cells, causing covalent bonds to form between adjacent thymine bases, producing thymidine dimers. Thymidine dimers do not base pair normally, which can cause distortion of the DNA helix, stalled replication, gaps, and misincorporation. These can lead to mutations, which can result in cancerous growths. However a positive effect of UVB light is that it induces the production of vitamin D in the skin.

Although, UVA is the least harmful, it can, however contribute to make photoaging (4), DNA damage and skin cancer. UVA has longer wavelength, so it can penetrate most windows. It also penetrates deeper into the skin comparing to UVB.

UVC rays are the most dangerous type of ultraviolet light but it has not been a factor to date in human cancers because it is sufficiently absorbed by the stratospheric ozone layer. Decreasing of the ozone and increasing holes in the ozone layer are, therefore, threats to living organisms on the planet.

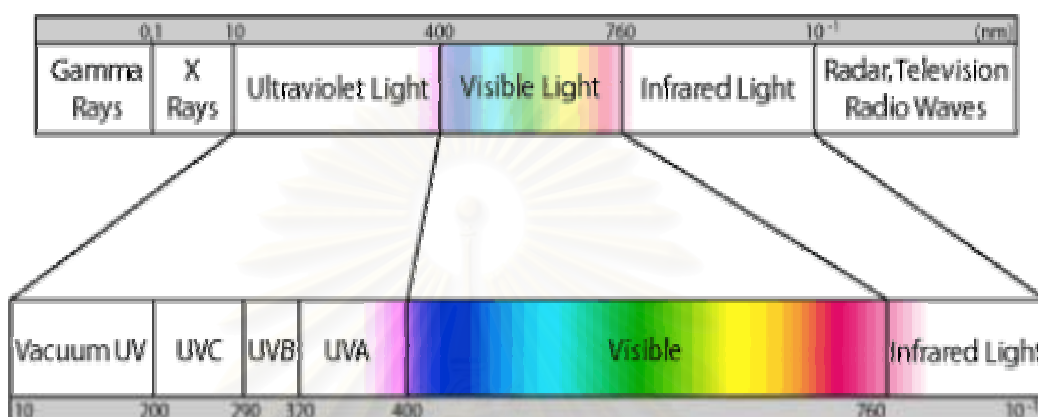


Figure 1.1 Electromagnetic spectrum

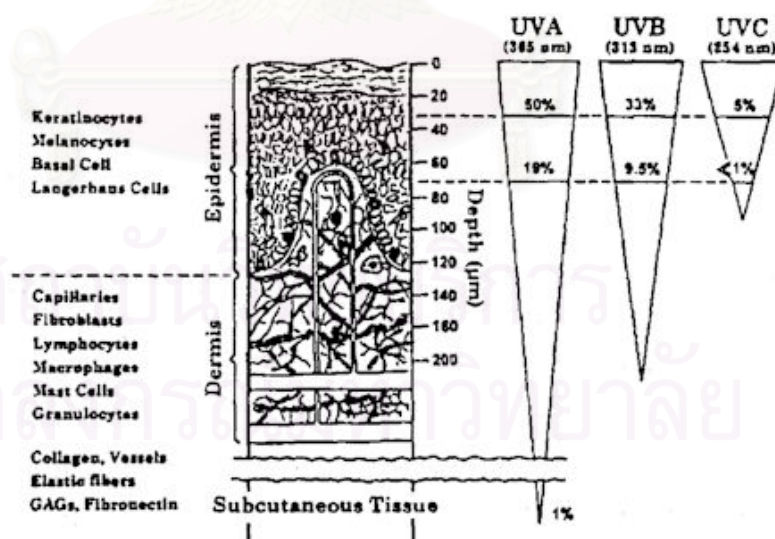


Figure 1.2 Depth of UV penetration into the skin

1.1.2 Protection

Photoprotection is the use of physical and/or chemical agents to prevent the skin-damaging effects of ultraviolet radiation. Physical agents are clothing, glasses, umbrellas and hats, awnings and tents those protect you from the sun when you are outdoors. Chemical agents are sunscreens you apply to your skin to protect the skin from UV radiation.

Now sunscreens those partly block UV are widely available and can be easily used for UV protection. An effective sunscreen should be broad-spectrum, providing protection against both the A and B wavelengths of UV.

1.2 Sunscreen Chemicals

1.2.1 Classification of Sunscreen Chemicals (5)

Sunscreens have traditionally been divided into physical blockers and chemical absorbers on the basis of their mechanism of action.

1.2.1.1 Physical blockers site on the skin's surface and ideally they should not have the ability to be absorbed. Light is reflected away into the atmosphere similar to a mirror or tin foil. Recent research indicates that the newer micro sized forms of physical blockers may also function in part by absorption. Popular physical blockers include two agents: zinc oxide and titanium dioxide. They are currently being used in conjunction with chemical absorbers to achieve high sun protection factors (SPF). Concerns on photocatalytic properties of these physical blockers have been a recent topic of discussion and research. (6-8)

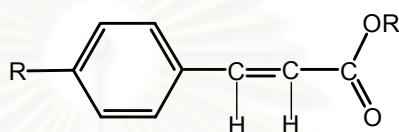
1.2.1.2 Chemical Absorbers (5, 9) generally aromatic compounds conjugated with a carbonyl group. These chemicals absorb high-intensity UV rays. Upon UV-absorption, electronic transitions within the molecules occur resulting in electronically excited molecules. For most sunscreen molecules, electrons in the excited state return to their ground state and radiate out the absorbed energy in the form of IR radiation.

UVA absorbers are chemicals those absorb radiation in the 320-360 nm regions of the UV spectrum. Examples of UVA absorbers include benzophenone and dibenzoylmethane.

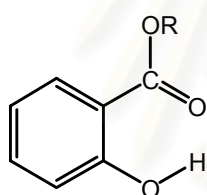
UVB absorbers are chemicals those absorb radiation in the 280-320 nm regions of the UV spectrum. Examples of UVB absorbers include salicylate, cinnamate and camphor derivatives.

The chemical absorbers used in sunscreen industry, can be classified into 7 categories (Figure. 1.3):

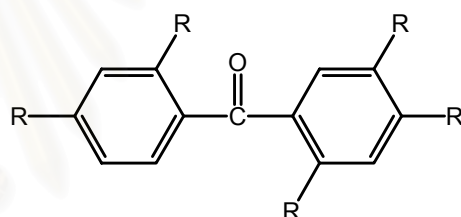
- A. cinnamate derivatives
- B. salicylate
- C. benzophenone
- D. camphor derivatives
- E. dibenzoylmethane



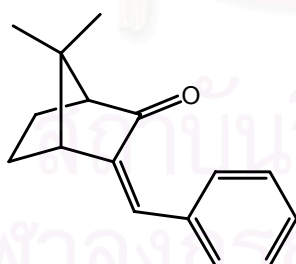
A. Cinnamate derivative



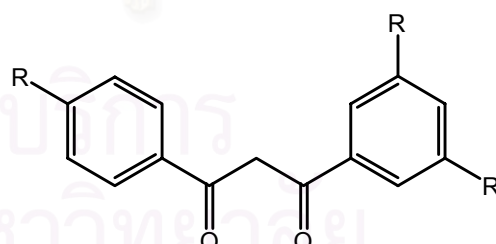
B. Salicylate



C. Benzophenone



D. Camphore derivatives



E. Dibenzoylmethane

Figure 1.3 Structures of the commonly used UV filters

1.2.2 Sunscreen Chemical Characters (10)

1.2.2.1 Absorption Range

Good sunscreen chemicals have to absorb the radiations in the ranges those harmful to human. Practically a choice is made between one or more sunscreens. As a result, a certain bandwidth filter usually corresponds to a combination of a few chemicals.

1.2.2.2 Solubility

Whether a sunscreen is oil based or aqueous gel, the chosen sunscreen compound must be compatible with its base. In the case of emulsion sunscreen, either water or oil soluble compounds can be used. Often a combination of water and oil soluble sunscreen is desirable due to cost and effectiveness considerations.

1.2.2.3 Sun Protection Factor (SPF)

SPF is a ratio of the amount of UVB radiation that produce erythema in skin covered by sunscreen to the amount of UVB radiation that produce a similar erythema in skin uncovered by sunscreen. The SPF value corresponds to the ability of sunscreen to protect against UVB radiation.

1.3 Mechanism of Organic UV Filters

Organic UV filters are generally aromatic compounds conjugated with a carbonyl group. In many examples, an electron releasing group such as an amine or a methoxy group is substituted in the *ortho* or *para* position of the aromatic ring. They absorb the harmful UVB rays (280-390 nm) and convert the absorbed energy into longer wave radiation (lower energy, $\lambda > 700$ nm). The process of sunscreen action is called “photophysical process”, not a photochemical process and ideally no change in molecular structure should be observed. Mechanism of sunscreen action (Figure 1.4) involves excitation of electron from ground state by absorbing the UV rays. Then upon the return of electron from excited state, the absorbed energy is emitted in the form of IR or heat. Various mechanism of energy release can be found in sunscreen molecules, e.g., vibrational relaxation, fluorescence and charge-transfer.

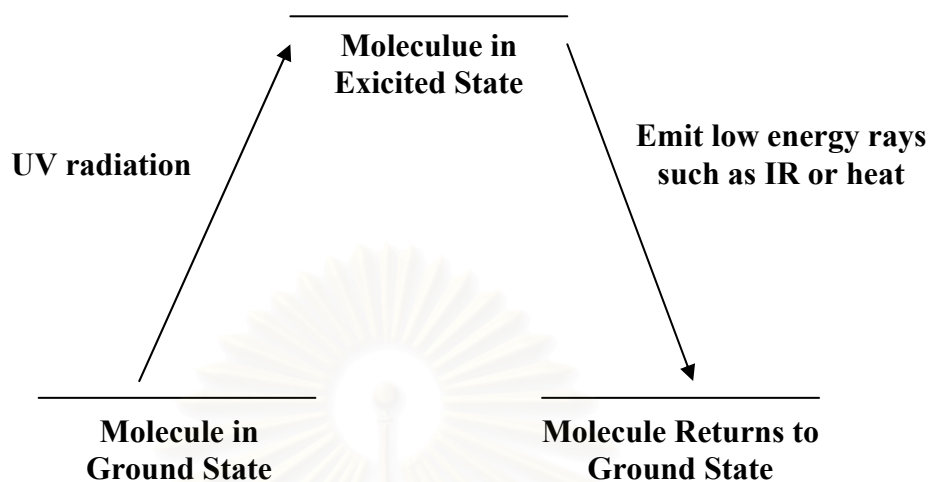


Figure 1.4 Mechanism of sunscreen action

Sunscreen preparations are usually applied superficially to large skin areas. Therefore, effectiveness implies that sunscreen filters adhere to skin like a protective film. They should have a high affinity for the stratum corneum. The UV filters are designed to remain on the uppermost layers of the skin; penetration through the skin should be low. (11, 12) ideal sunscreen products should exhibit high skin accumulation of UV absorbers with minimal permeation to the systemic circulation. (13)

สถาบันวิทยบริการ
จุฬาลงกรณ์มหาวิทยาลัย

1.4 Octyl Methoxycinnamate (OMC)

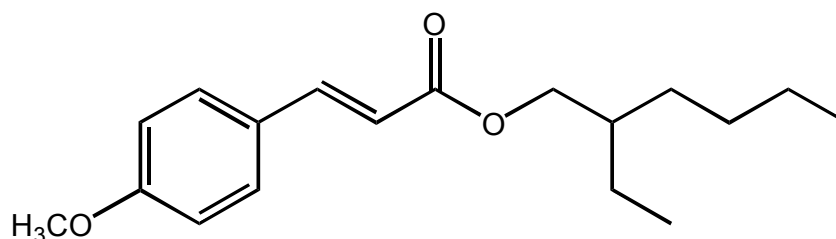


Figure 1.5 Structure of Octyl methoxycinnamate (OMC)

Octyl methoxycinnamate (OMC, Figure 1.5) is today the most common organic UVB filter being used in the world. The compound has been one of the most frequently used sunscreen ingredient in a variety of cosmetic products for decades. OMC is a cinnamic acid derivative that has a methoxy group on the *para* position and is esterified with 2-ethylhexanol; the chemical name is 2-ethylhexyl-3-(4-methoxyphenyl)-2-propenoate.

Many research groups have demonstrated that OMC is quite safe concerning allergic contact (AC) and photoallergic (PA) effects of the compound. (14-15) However, many reports have shown that substantial amount of applied cinnamate derivatives, can be absorbed through human's skin layer. (16-17) For example, in 1997 C.G.J. Hayden and coworkers (16) could recover OMC from volunteers' breast milk. Benech-Kieffer, F. and coworkers (17) demonstrated that OMC was absorbed though both pig- and human-skin.

Besides the absorption problem, photostability (refers to the ability of a molecule to remain intact upon being irradiated) is potentially a problem with OMC. Many reports had addressed this problem. (18-20) For example, in 1990 N.A. Shaath and coworkers (18) studied the stability of various UV filters under UV light. They found that OMC has moderate degradation in mineral oil. In 1995 J. Meijer and M. Londen (19) studied the stability of OMC in an ordinary sun lotion using HPLC. The reverse phase HPLC revealed a new peak with slightly lower retention time after OMC was exposed with the sunlight. This new peak was dramatically increased while the OMC peak was significantly decreased after more light exposure. Similarly, in 1999 N. Tarras-Wahlberg and coworkers (20) reported that octyl dimethyl PABA,

butylmethoxy dibenzoylmethane and OMC were not stable against UV irradiation. In 2001, Pattanaargson and Limpong (21) isolated the pure photo-degradation product of OMC after light exposed by HPLC. They found for the first time that the isolated photo-degradation product of *E*-OMC was *Z*-OMC. Moreover, in 2004, Pattanaargson and coworkers (22) demonstrated that a *trans*-(*E*) to *cis*-(*Z*) configurational change of OMC occurred upon light exposure (Figure 1.6). In this work, they showed that photostationary equilibrium between *E* and *Z* configuration varied with concentration of OMC and the type of solvent used. In addition they obtained the molar absorption coefficient value of *Z*-OMC about 12,000 (comparing to 21,000 for the *E*-OMC).

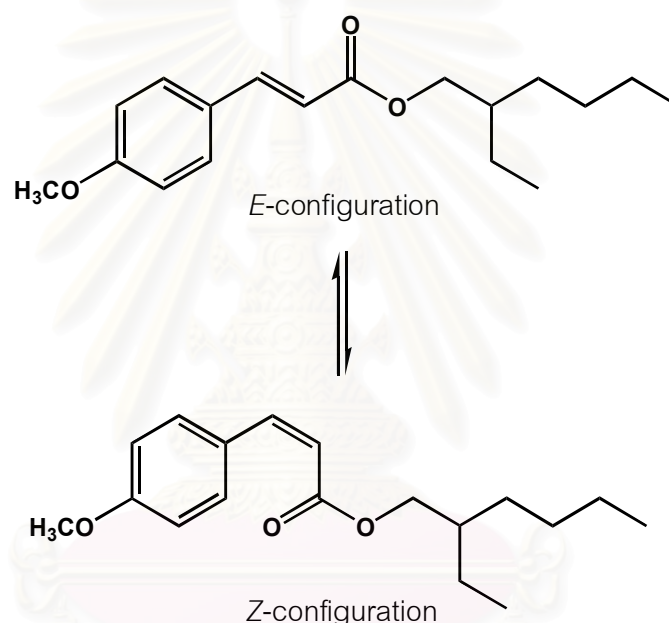


Figure 1.6 Conversion of *E*-OMC to *Z*-OMC after exposure to UV radiation

Since all of the above mentioned works on OMC photoisomerization were done in solution, therefore, *E-Z* isomerization of OMC on surface still could not be predicted effectively. Moreover, since the use of OMC is on skin surface, it will, therefore, be very useful to know the photoisomerization behavior of this compound on surface. However, techniques used in previous works such as NMR, UV-absorption spectrophotometry, and HPLC, cannot be applied to *in situ* monitoring of molecular changes on the surface. As a result, this research has explored the use of ATR-FTIR spectroscopy for evaluating the photostability of OMC on surface. In particular, photoisomerization of OMC on surface was studied using ATR-FTIR.

1.5 Attenuated Total Reflectance Fourier Transform Infrared (ATR-FTIR) Spectroscopy

Attenuated Total Reflectance Fourier transform infrared (ATR-FTIR) spectroscopy is today the most widely used FT-IR sampling tool. ATR-FTIR was developed by Harrick and Fahrenfort in the 1960's. (23) ATR generally has been employed for various applications such as qualitative or quantitative analyses of samples with little or no sample preparation. The advantage of ATR sampling comes from the very thin sampling path length. In other words, the depth of penetration of the IR beam into the sample is small. This is in contrast to traditional FT-IR sampling by transmission where the sample must be diluted with IR transparent medium, pressed into a pellet or pressed to a thin film, prior to analysis.

1.5.1 Information provided from ATR-FTIR spectrometry

In the mid-infrared, absorption of radiation is related to fundamental vibrations of the chemical bonds. Internal reflection infrared spectrometry provides information related to the presence or absence of specific functional groups and the chemical structure of membrane/surface. Shifts in the frequency of absorption bands and changes in relative band intensities indicate changes in the chemical structure of the sample or change in the environment of the analyzed surface.

ATR-FTIR spectrometry can also be used to determine changes in surface chemistry after special chemical or physical treatments such as exposure to light and thermal annealing. Furthermore it can also be used to identify unique features on the membrane/surface after chemical surface modification.

1.5.2 Principle of the ATR Technique

Internal reflection spectrometry or attenuated total reflectance infrared (ATR-FTIR) spectroscopy can provide valuable information related to the chemical structure of membrane layers. Mid-infrared spectra are obtained by pressing small pieces of membrane against an internal reflection element (IRE). The infrared radiation is, then, coupled in to the IRE in order to acquire chemical information at the surface.

IRE is an essential part of ATR accessories. It usually is made of infrared transparent material with high refractive index. The common IRE configurations used for experimental ATR setup include variable-angle hemispherical crystals with single reflection or multiple-reflection planar crystals (24) (Figure 1.7).

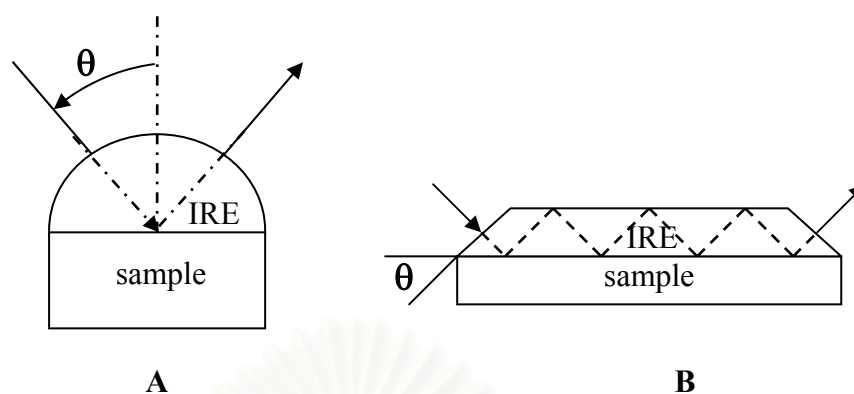


Figure 1.7 The common IRE configurations: (A) single-reflection variable angle hemispherical crystal and (B) multiple-reflection planar crystal.

For the multiple-reflection planar crystal, IR radiation is focused onto an end of the IRE. Light enters the IRE and reflects down the length of the crystal. At each internal reflection, the IR radiation penetrates a short distance (~ 1 mm) from the surface of the IRE into the membrane (Figure 1.8). It is this unique physical phenomenon that enables one to obtain infrared spectra of samples placed in contact with the IRE.

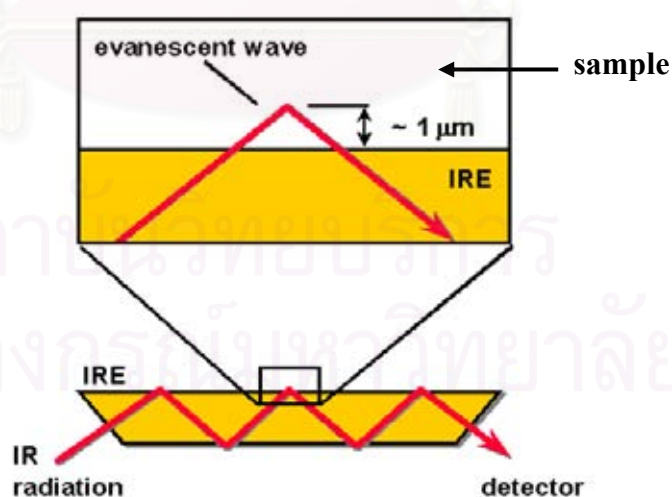


Figure 1.8 Total internal reflection at the interface of an internal reflection element. Depth of penetration of the evanescent wave is approximately $1 \mu\text{m}$.

For the analysis of solid sample, it is necessary to have good contact between the sample and the IRE. The accessories have devices to clamp the sample to the crystal surface with some applied pressure in order to ensure a good contact.

1.5.3 ATR crystal materials and accessories

There are several crystal materials available for ATR. The selection of the ATR crystal varies with the type of samples. Selection can be made to control a depth of IR beam penetration. Hardness and pH of sample must be considered as to prevent crystal damage. Since there are various crystal plates, ATR-FTIR can be applied to a wide range of applications. Table 1.2 provides some guidelines for selection of ATR crystal.

Table 1.2 ATR Crystal Properties.

Crystal	n_1	d_p , for $n_2= 1.5$ $\lambda= 1000 \text{ cm}^{-1}$ @ 45 deg	Water Solubility (g/100g)	pH Range	Hardness (Kg/mm ²)
AMTIR	2.5	1.46	Insoluble	1-9	170
Diamond	2.4	1.66	Insoluble	1-14	5,700
Germanium	4.0	0.65	Insoluble	1-14	550
KRS-5	2.4	1.73	0.05	5-8	40
Silicon	3.4	0.84	Insoluble	1-12	1,150
ZnS	2.2	2.35	Insoluble	5-9	240
ZnSe	2.4	1.66	Insoluble	5-9	120

n_1 : refractive index of crystal

AMTIR : Amorphous Material Transmitting IR

n_2 : refractive index of sample

KRS-5 : Thallium Bromo-Iodide

d_p : penetration depth

Zinc Selenide (ZnSe) (see Figure 1.9) and Germanium (Ge) are the most common crystals used for ATR sampling. ZnSe is ideal for analyzing liquids, non-abrasive pastes and gels. It is considered not very robust and has a working pH range of 5-9. ZnSe can be scratched quite easily therefore care must be taken during cleaning. It is recommended that lint free tissue is used. (25) For Germanium, it has a much better working pH range and can be used to analyze weak acids and alkalis. It has the highest refractive index among all the available ATR materials.

Similar to all FT-IR measurements, an infrared background must be collected. In ATR-FTIR, the background is usually taken from the clean ATR crystal. The cleaning of ATR crystal surface is a necessary step to remove the contaminants on crystal before and after analyses. High volatility solvents can be used to wash the surface.



Figure 1.9 ZnSe crystal

1.5.4 Analyzing liquids

After the crystal has been cleaned and an infrared background has been collected, the liquid is simply poured onto the crystal. The whole crystal must be covered with liquid sample in order to perform a quantitative or qualitative analysis. The crystal is recessed into the metal plate to retain the sample. Pastes and other semi-solid sample can be readily measured by spreading them on the crystal. Horizontal ATR units are often used for quantitative work in preference to transmission cells because they are easier to clean.

1.6 Objective

1.6.1 Preparation of Z-OMC.

1.6.2 Study of *E*- to *Z*- and *Z*- to *E*-OMC photoisomerization on ZnSe.

1.6.3 Study of *E*- to *Z*-OMC photoisomerization on rat skin.



สถาบันวิทยบริการ
จุฬาลงกรณ์มหาวิทยาลัย

CHAPTER II

EXPERIMENT

2.1 Materials

Animal Treatment

Skin specimens of 3 weekolds mice (*Mus musculus* Linn.) were purchased from National Laboratory Animal Centre (Thailand). They were kept frozen at -20°C . Prior to experimentation the frozen skin was allowed to defrost at room temperature before being cut in to approximately $5.0 \times 0.5 \text{ cm}^2$ pieces.

UV lamp

For UV irradiation, a Daavlin Psorawand UV lamp: PW-UVB-220 was used (Daavlin, OH, USA) in all experiments. Its UVB light spectrum is depicted in Figure 2.1. Measuring of the UV irradiance of the lamp was done using UVB power meter: UVB-500c (National biological corporation, Twinsburg, Ohio, USA).

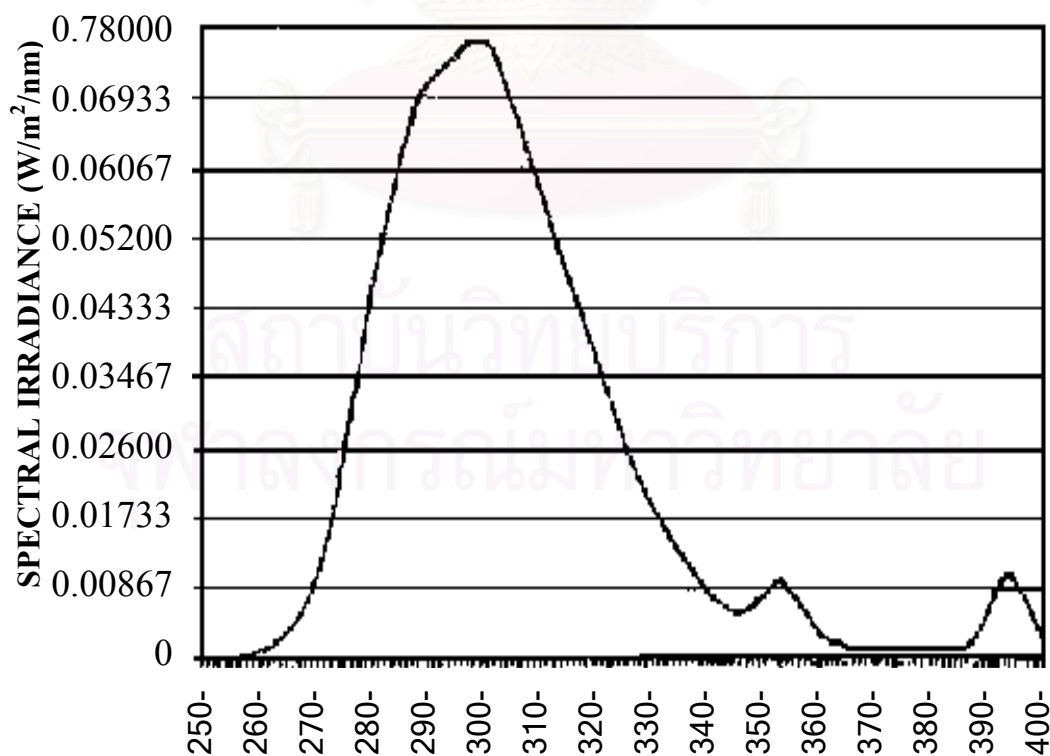


Figure 2.1 Radiation from the UVB lamp used in the experiment

2.2 Chemicals

Octyl methoxycinnamate (Eusolex[®] 2292) was obtained from Merck Co. Ltd. (Bangkok, Thailand) and was kept in a lightproof container at 0°C until use to insure no photoisomerization. Solvents used in spectroscopic works were reagent or analytical grades purchased from Labscan (Bangkok, Thailand). Solvents used in column chromatography were purified from commercial grade solvents prior to use by distillation.

2.3 Preparation of OMC solutions

2.3.1 Preparation of *E*-OMC solutions

Stock *E*-OMC solutions of 1.70×10^{-3} , 3.40×10^{-3} , 6.90×10^{-3} , 1.03×10^{-2} , 1.72×10^{-1} , 3.44×10^{-1} and 6.89×10^{-1} M were prepared in methanol (see Table 2.1 for unit conversion) using standard *E*-OMC (Eusolex[®] 2292). The solutions were kept in lightproof container at room temperature. These solutions were used in *E-Z* photoisomerization study.

Table 2.1 Concentration of prepared OMC solution

Concentration		
mol/L	g/L	ppm
1.70×10^{-3}	0.5000	5.00×10^2
3.30×10^{-3}	0.9720	9.72×10^2
3.40×10^{-3}	1.000	1.00×10^3
6.90×10^{-3}	2.000	2.00×10^3
1.03×10^{-2}	3.000	3.00×10^3
1.72×10^{-1}	50.00	5.00×10^4
3.44×10^{-1}	100.0	1.00×10^5
6.89×10^{-1}	200.0	2.00×10^5

2.3.2 Preparation of Z-OMC

The solution of 6.90×10^{-3} M (2000 ppm) *E*-OMC in methanol was irradiated for 168 h with a Daavlin Psorawand UV lamp (at 0.08 mW/cm^2). The light exposed solution was then evaporated under vacuum at 50°C by rotary evaporation. The residue was then separated by column chromatography to isolate the *Z*-OMC out from the mixture of *E*-OMC and *Z*-OMC.

The column used was a glass column packed with Octadecyl-functionalized silicagel, C-18 (Sigma-Aldrich Chemie GmbH, Steinheim, Germany). Two grams of the residue (mixture of *E*-OMC and *Z*-OMC) were loaded onto the column. Gradient elution was done as the following order; methanol:water (70:30 (v/v)), methanol:water (80:20 (v/v)), methanol:water (90:10 (v/v)) and pure methanol. TLC was used for determination of the first eluted fraction and NMR was used to analyze each fraction. Then all the *Z*-OMC fractions were pooled together and immediately evaporated under vacuum by rotary evaporation at 50°C . Care was given to prevent light exposure to every eluted fraction.

2.3.3 Preparation of *E*-OMC and *Z*-OMC for calibration standard and for *Z* to *E* photoisomerization

The 3.30×10^{-3} M *E*-OMC solution was prepared by dissolving 0.0243 g (8.37×10^{-5} mol) of *E*-OMC in methanol and the final volume was adjusted to 25 mL. *Z*-OMC solution of the same concentration was also prepared similarly using isolated *Z*-OMC obtained from section 2.2.2.

The binary-phase calibration standard sets consisting of *E*-OMC and *Z*-OMC as shown in Table 2.2 were created. All the standards prepared were kept away from light.

Table 2.2 shows volumes of 3.30×10^{-3} M *E*-OMC and 3.30×10^{-3} M *Z*-OMC used in preparing calibration standards.

Ratio <i>E</i>:<i>Z</i> (v/v)	<i>E</i>-OMC (mL)	<i>Z</i>-OMC (mL)
100:0	1.00	0.00
90:10	0.90	0.10
75:25	0.75	0.25
50:50	0.50	0.50
25:75	0.25	0.75
10:90	0.10	0.90
0:100	0.00	1.00

2.4 Nuclear magnetic resonance (NMR) spectroscopy

The ^1H -NMR spectra were recorded on ACF 200 Spectrometer which operated at 400.00 MHz (Varian Company, CA, USA). Chemical shifts are reported in ppm (δ) relative to TMS.

Samples were solubilized at a concentration of ca. 10 mg/mL in deuterated chloroform (CDCl_3) before subjecting NMR spectroscopy.

2.5 Attenuated Total Reflection Fourier Transform Infrared (ATR-FTIR) Spectroscopy

Spectral acquisition

IR spectra were obtained using a Nicolet Magna-IR[®] 750 FT-IR spectrometer equipped with a DTGS detector. Spectra were acquired at a resolution of 4 cm^{-1} with 64 scans at the wavelength of $4000\text{--}650 \text{ cm}^{-1}$.

The spectrometer was linked to a PC equipped with Nicolet's OMNIC software package Version 5.1 (Nicolet Instrument Corporation, WI, USA) to allow

the automated collection of IR spectra. The transmission mode was used for all measurements. All experiments were done at ambient temperature, $25\pm 2^\circ\text{C}$. Experiments were done either in duplicate or triplicate. The experiments were done using either single reflection system or multiple reflection system.

2.5.1 Single Reflection System

Experiments involving comparison peak area of those *E*- and *Z*-OMC were done with single reflection system in which the variable angle reflection accessory (the SeagullTM, Harrick Scientific, U.S.A.) with a hemispherical ZnSe (Figure 2.2) were employed.

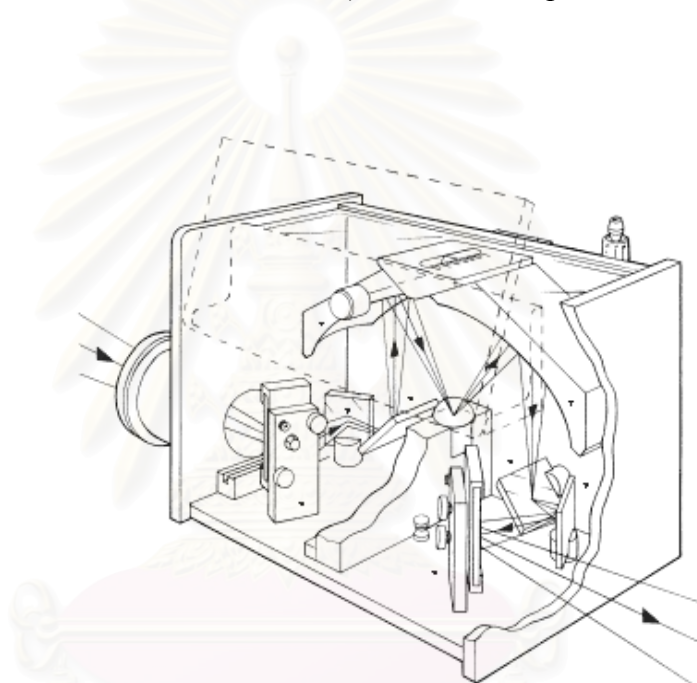


Figure 2.2 The SeagullTM Variable Angle Reflection Attachment.

To obtain IR spectra of the *Z*-OMC, pure *Z*-OMC collected from the column chromatography was dropped onto the SeagullTM accessory and the spectra were recorded and processed using OMNIC 5.1 software. Similar experiment was done to standard *E*-OMC to obtain IR spectrum of the *E* configuration.

2.5.2 Multiple Reflection System

Kinetic studies of *E* to *Z* and *Z* to *E* photoisomerization of OMC were all done using multiple reflection system in which the multiple attenuated total reflectance accessory (MATR) was mounted into the sample compartment. The internal reflection

crystal (Spectra Tech, USA), which was made of zinc selenide (ZnSe), was set at a 45 degree the angle between incidence beam and the detected IR beam.

2.5.2.1 Kinetic study of *E to Z* Photoisomerization on ZnSe

For the first spectrum, a specific amount of *E*-OMC solutions was dropped over the surface of a ZnSe crystal (surface area = $5.0 \times 0.5 \text{ cm}^2$) using an analytical syringe and was spread evenly over the surface. This spread solution was dried under ambient condition for at least 5 min. The amounts of solution used were 0.50 mL (for concentration of 1.70×10^{-3} , 3.40×10^{-3} , 6.90×10^{-3} and 1.03×10^{-2} M), 0.050 mL (for concentration of 1.72×10^{-1} , 3.44×10^{-1} and 6.89×10^{-1} M) and 0.1 mL (for concentration of 3.30×10^{-3}). The final coverage on ZnSe surface was listed in Table 2.3. Then this ZnSe crystal was installed into the sample cell. The IR scan was done between 4000 and 650 cm^{-1} with 4 cm^{-1} resolution. Each spectrum obtained was a result of 64 scans.

Table 2.3 Dispersion of OMC on ZnSe's surface area $5.0 \times 0.5 \text{ cm}^2$

Concentration		Dispersion on ZnSe ($5.0 \times 0.5 \text{ cm}^2$)	
mol/L	ppm	mg/cm ²	mol/cm ²
1.70×10^{-3}	5.00×10^2	1.00×10^{-1}	3.44×10^{-7}
3.30×10^{-3}	9.72×10^2	3.89×10^{-2}	1.34×10^{-7}
3.40×10^{-3}	1.00×10^3	2.00×10^{-1}	6.89×10^{-7}
6.90×10^{-3}	2.00×10^3	4.00×10^{-1}	1.38×10^{-6}
1.03×10^{-2}	3.00×10^3	6.00×10^{-1}	2.04×10^{-6}
1.72×10^{-1}	5.00×10^4	1.00	3.44×10^{-6}
3.44×10^{-1}	1.00×10^5	2.00	6.89×10^{-6}
6.89×10^{-1}	2.00×10^5	4.00	1.38×10^{-5}

For the next spectra, the irradiation unit was setup as shown in Figure 2.3. UV-Irradiation was performed with a UVB lamp. The UVB light was focused on the surface of the ZnSe. The UV exposure time was 1 min. Immediately after exposure, IR-acquisition was done to the sample. Then the UV-light exposure and the IR-recording steps were repeated for a total of 10 cycles (total exposure time of 10 min). After 10 min UV-exposure time, the steps were repeated again but the UV-exposure time was now changed from 1 min to 5 min. The repeat of 5 min UV-exposure and IR-recording was done for 10 cycles (total UV exposure time of $10 \times 5 = 50$ min).

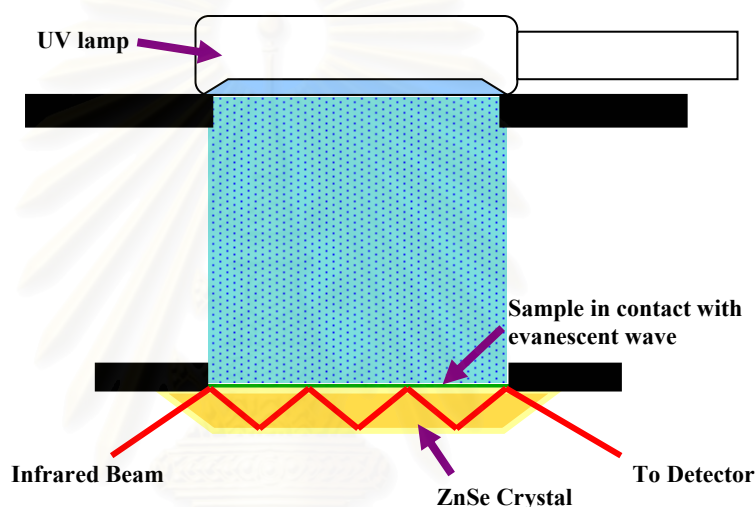


Figure 2.3 The layout of the irradiation unit

2.5.2.2 Kinetic study of *E* to *Z* photoisomerization on rat skin

A specific amount of *E*-OMC solution was dropped over the surface of a skin specimen (surface area = 5.0×0.5 cm²) using an analytical syringe. The solution was then spread evenly over the skin surface. Then it was dried under ambient condition for at least 5 min. The amount of the OMC solution used was 0.050 mL (for concentration of 1.72×10^{-1} , 3.44×10^{-1} and 6.89×10^{-1} M). The rat skin specimens were then fixed on ATR clamp accessories as shown in figure 2.4. The first IR spectrum was recorded and processed. No UV radiation was done on this first sample acquisition. After the spectrum of the unexposed sample was collected, the sample cell was opened and the UV-light was applied directly to the sample piece. The UV exposure time was 1 min. Immediately after exposure, IR-acquisition was done to the sample. Then the UV-light exposure and the IR-recording steps were repeated for a

total of 10 cycles (total exposure time of 10 min). After 10 min of UV-exposure time, the steps were repeated again but the UV-exposure time was now changed from 1 min to 5 min. The repeat of 5 min UV-exposure and IR-recording was done for 10 cycles (total UV exposure time of $10 \times 5 = 50$ min).



Figure 2.4 Instrumental setup for kinetic studies on rat specimens

2.5.2.3 Kinetic study of *Z* to *E* photoisomerization on ZnSe

The *Z*-OMC solution (972 ppm, 3.30×10^{-3} M) was spread over the surface of a skin specimen (surface area $= 5.0 \times 0.5$ cm²) and left dry as previously described. The volume of solution used was 0.10 mL. The first IR spectrum was recorded without UV radiation to the sample as described previously. After the unexposed IR spectrum was recorded, similar IR-spectrum of UV-exposed samples were recorded as described previously using similar UV-exposure cycles.

2.5.2.4 Binary-phase calibration standards

The 0.10 mL of binary-phase mixture of the *E*-OMC and the *Z*-OMC was dropped and spread over the surface of ZnSe (surface area $= 5.0 \times 0.5$ cm²). The IR spectra were then recorded and processed. A set of binary-phase calibration standards was analyzed in duplicate.

2.6 Data analysis

Each spectrum's baseline was adjusted prior to the integration of the interested peak area using OMNIC v.5.1 software. The interested peaks lie at 963-999 cm^{-1} (correspond to the $>\text{CH}=\text{CH}<$ bending of the *E* configuration, **b**) and at 998-1060 cm^{-1} (correspond to the C-O-C stretching; these were used as internal standard peaks, **a**).

The **b/a** ratio was then calculated by dividing the peak area of **b** by the **a** peak area. The graph between **b/a** ratio versus UV exposure time was then constructed. The least squared fit of the graph was then performed.



สถาบันวิทยบริการ
จุฬาลงกรณ์มหาวิทยาลัย

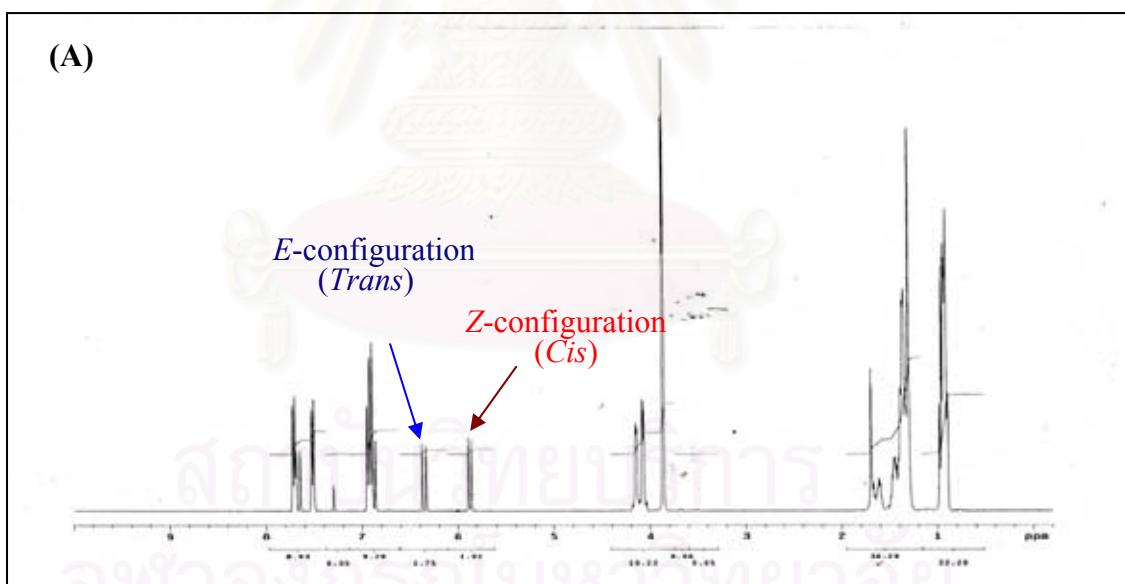
CHAPTER III

RESULTS AND DISCUSSION

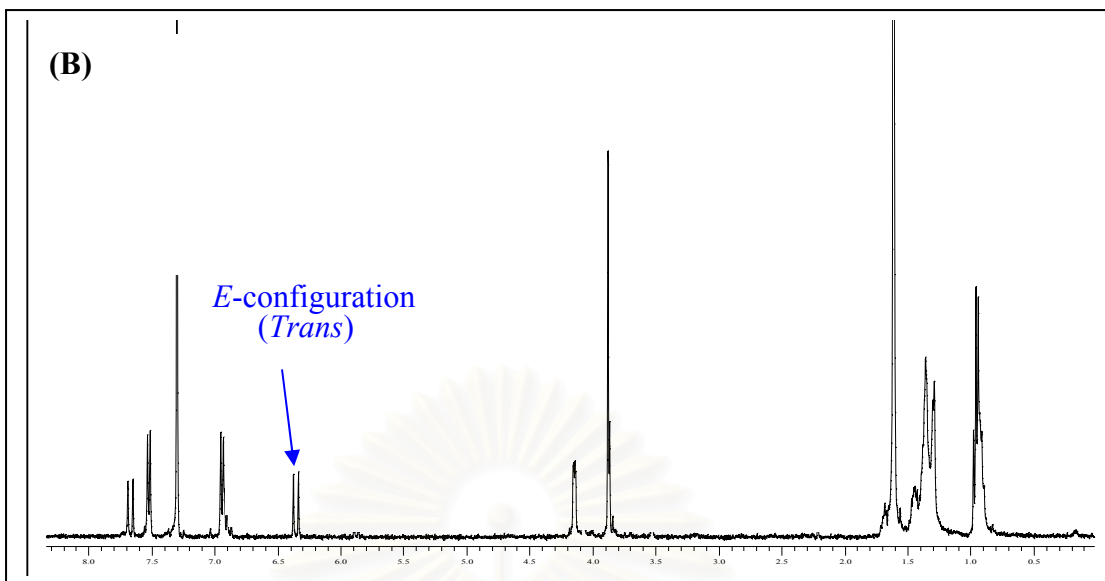
3.1 Purification of Z-OMC

As mentioned in chapter II that Z-OMC could be induced by exposing *E*-OMC solution to the UVB light, however, the Z-OMC formed was mixed with *E*-OMC in the solution. In this work we have used reverse phase column chromatography to separate the two isomers from each other. The pure Z-OMC (~2 g) could be obtained and the purity was checked with NMR. This Z-OMC was then used as calibration standard together with the commercially available *E*-OMC.

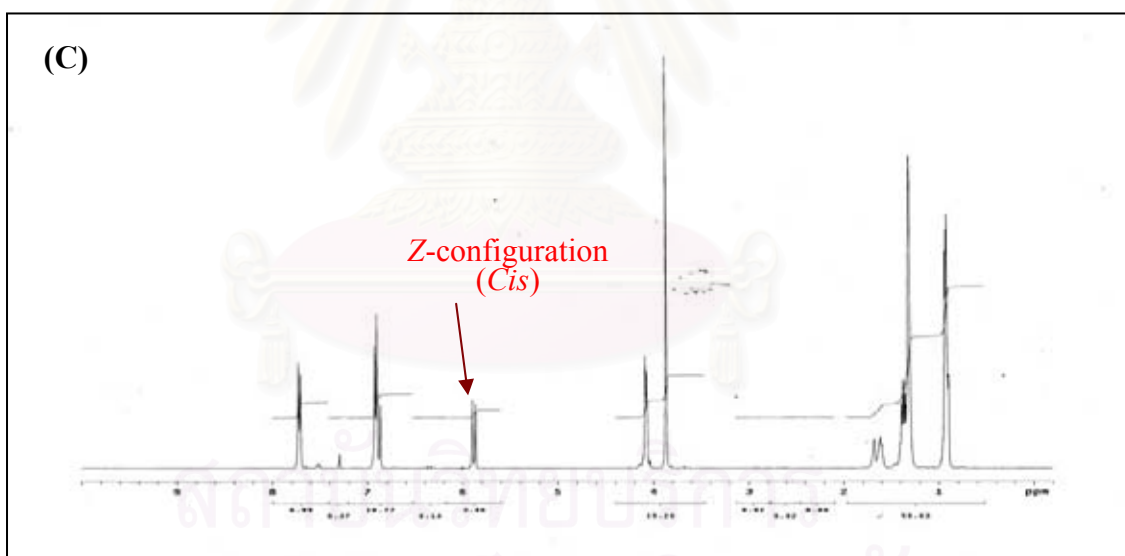
The $^1\text{H-NMR}$ analyses of the *E*- and *Z*- isomer showed a significant difference of a CH=CH resonances between the *E* and the *Z* configuration (Figure 3.1).



E-Z mixture (A): colorless oil, $^1\text{H-NMR}$ (CDCl_3) δ (ppm): 7.72(d, $J=8.6$ Hz, 2H, Ar-H of the Z-OMC), 7.67 (d, $J=15.6$ Hz, 1H, *trans* Ar-CH=), 7.52 (d, $J=8.6$ Hz, 2H, Ar-H of the *E*-OMC), 6.94 (d, $J=8.6$ Hz, 2H, Ar-H of the *E*-OMC), 6.91 (d, $J=8.6$ Hz, 2H, Ar-H of the Z-OMC), 6.88 (d, $J=13.3$ Hz, 1H, *cis* Ar-CH=), 6.36 (d, $J=16.3$ Hz, 1H, *trans* =CH-COOR), 5.88 (d, $J=12.5$ Hz, 1H, *cis* =CH-COOR), 4.14 (d, $J=5.7$ Hz, 2H, $-\text{OCH}_2$ of the *E*-OMC), 4.07 (d, $J=5.7$ Hz, 2H, $-\text{OCH}_2$ of the Z-OMC), 3.88 (s, 3H, OCH_3 of the *E*-OMC), 3.86 (s, 3H, OCH_3 of the Z-OMC) and 1.70-0.93 (m, 15H, $-\text{C}_7\text{H}_{15}$).



E-OMC (B): colorless oil, $^1\text{H-NMR}$ (CDCl_3) δ (ppm): 7.67 (d, $J=16.0$ Hz, 1H, Ar-CH=), 7.52 (d, $J=8.6$ Hz, 2H, Ar-H), 6.94 (d, $J=8.6$ Hz, 2H, Ar-H), 6.36 (d, $J=16.3$ Hz, 1H, =CH-COOR), 4.16 (d, $J=5.7$ Hz, 2H, -OCH₂), 3.81 (s, 3H, OCH₃), and 2.21-1.25 (m, 15H, -C₇H₁₅).



Z-OMC (C): colorless oil, $^1\text{H-NMR}$ (CDCl_3) δ (ppm): 7.72 (d, $J=8.6$ Hz, 2H, Ar-H), 6.91 (d, $J=8.8$ Hz, 2H, Ar-H), 6.88 (d, $J=13.3$ Hz, 1H, *cis* Ar-CH=), 5.88 (d, $J=12.5$ Hz, 1H, =CH-COOR), 4.08 (d, $J=5.7$ Hz, 2H, -OCH₂), 3.86 (s, 3H, OCH₃), and 1.70-0.93 (m, 15H, -C₇H₁₅).

Figure 3.1 $^1\text{H-NMR}$ of a mixture of *E*- and *Z*-OMC (light exposed OMC solution)
(A), standard *E*-OMC (B), isolated *Z*-OMC (C)

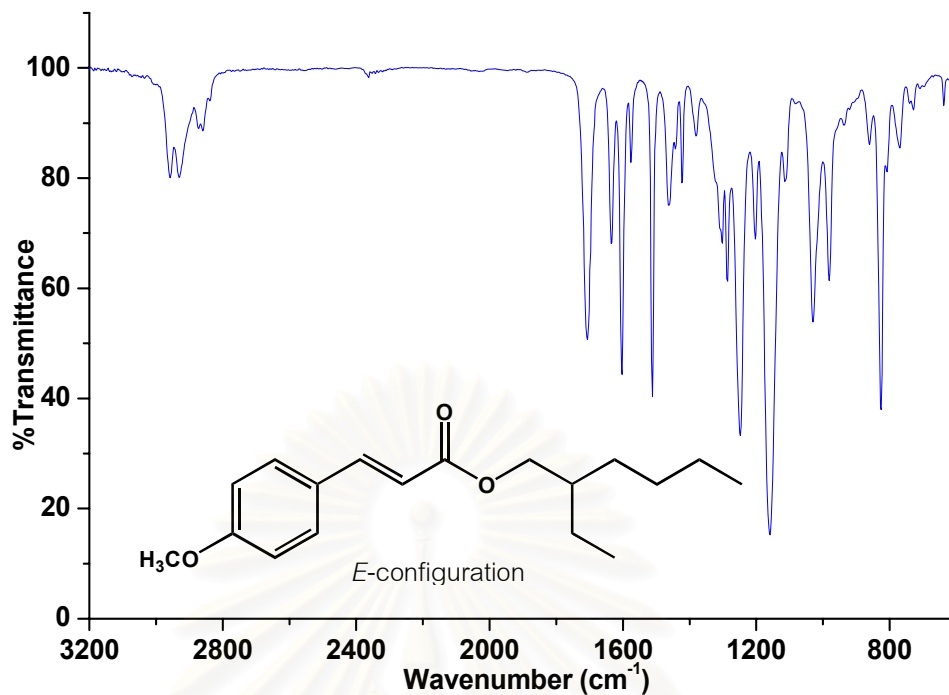


Figure 3.2 Spectrum of *trans*-OMC (*E*-OMC) in the frequency range of 3200-600 cm⁻¹.

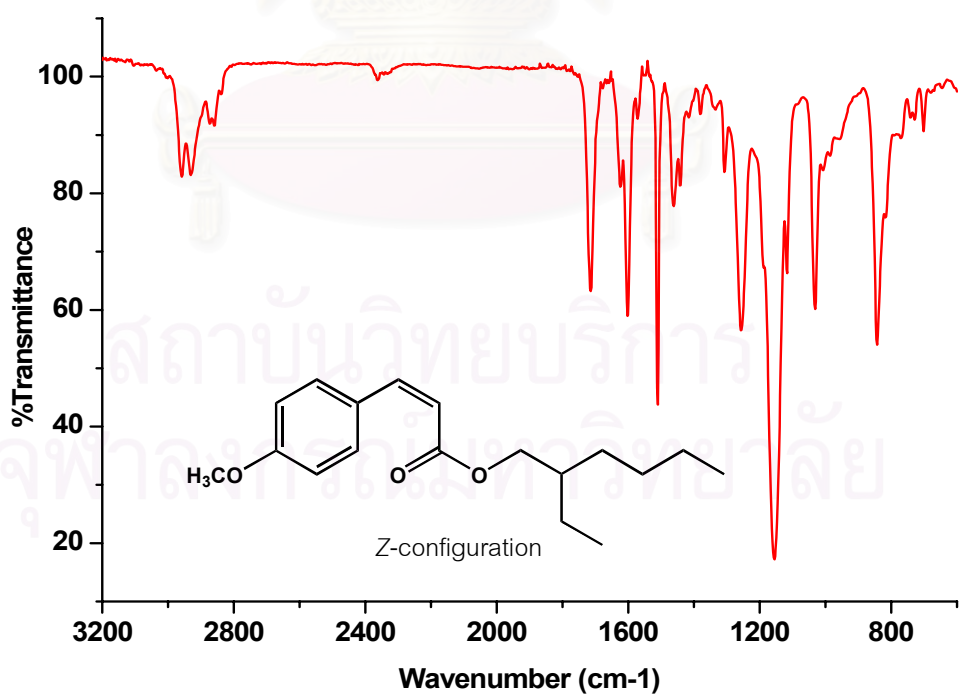


Figure 3.3 Spectrum of *cis*-OMC (*Z*-OMC) in the frequency range of 3200-600 cm⁻¹.

In order to monitor the change from *E*- to *Z*-OMC or from *Z*- to *E*-OMC, major differences between the IR spectrum of the *E* and that of the *Z* must be identified. Figure 3.2 and 3.3 shows ATR-FTIR spectra of *E*-OMC and *Z*-OMC, respectively. Figure 3.4 shows the two spectra in stacked layout for easy comparison. Assignments of the IR peaks are demonstrated in Table 3.1. The CH stretching vibrational bands were observed in the region of 2800-3100 cm^{-1} . These medium to strong intensity bands are in the region expected for saturated (<3000) and unsaturated (>3000) hydrocarbons. The carbonyl group exhibits a strong absorption band due to C=O stretching vibration and is observed at 1700-1720 cm^{-1} . In this case, the frequency observed was lower than normal ester because of aryl group conjugation. The *E* and the *Z* configuration showed different C=C (from Ph-CH=CH-) stretching, i.e. 1665-1635 cm^{-1} for *E*-OMC and 1635-1610 cm^{-1} for *Z*-OMC. Figure 3.5 shown expansions of IR spectra in these regions.

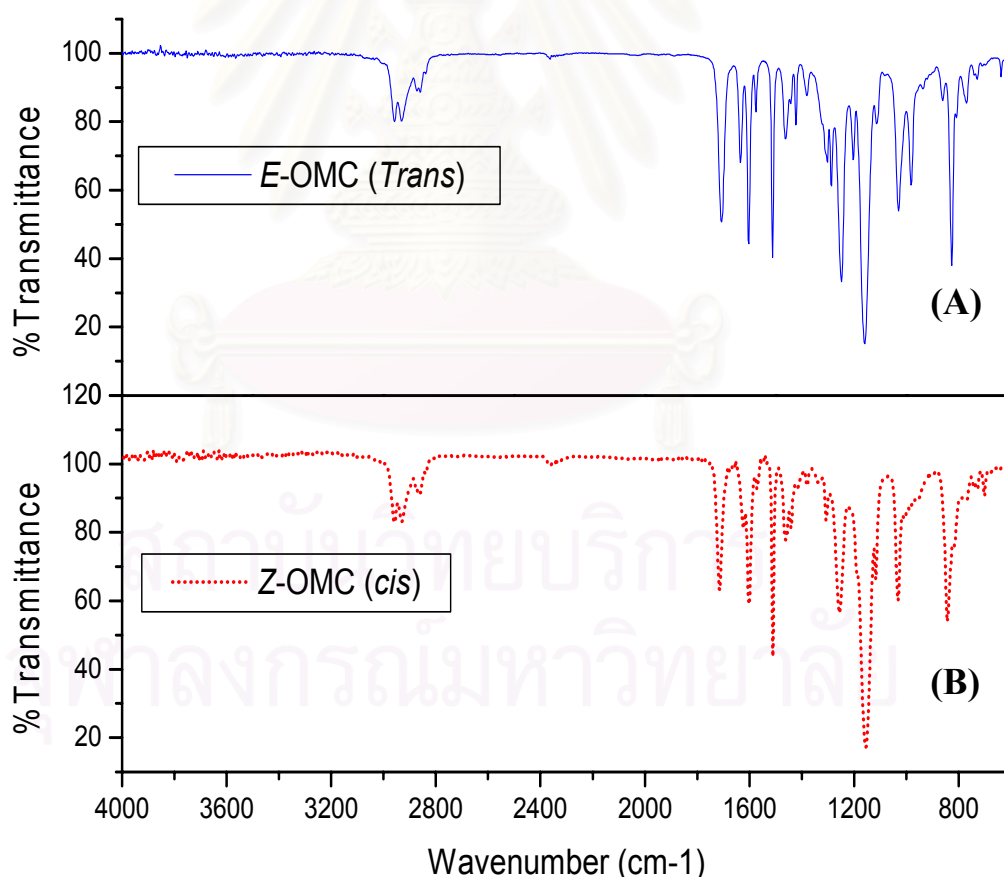


Figure 3.4 ATR-FTIR spectra of *E*-OMC (A) and *Z*-OMC (B).

Table 3.1 Vibrational spectral assignments of OMC in the Infrared (26)

Group or Class	Frequency Ranges(cm^{-1}) and Intensities	Assignment and remarks
Vinylene	3040-3010 (m) 1635-1610 (w-m) 1665-1635 (w-m) 730-665 (s) 995-950 (s)	= CH ₂ stretching C= C stretch (<i>Z</i> -configuration (<i>cis</i>)) C= C stretch (<i>E</i> -configuration (<i>trans</i>)) CH out-of-plane deformation (<i>Z</i> -configuration (<i>cis</i>)) CH out-of-plane deformation (<i>E</i> -configuration (<i>trans</i>))
Esters	1720-1700 (vs) 1260-1150 (vs) 645-575 (s)	C= O stretch C- O- C antisym stretch O-C-O bend
Aromatic compounds	2980-2850 (m) 2000-1660 (w) 1630-1430 (variable) 900-650 (s) 580-420 (m-s)	CH stretch, several peak Overtone and combination bands Aromatic ring stretching (four bands) out-of-plane CH deformations ring deformations (two bands)
Alkyl	2980-2850 (m) 1470-1450 (m) 1400-1360 (m) 740-720 (w)	CH stretch ,several bands CH ₂ defomation CH ₃ defomation CH ₂ rocking

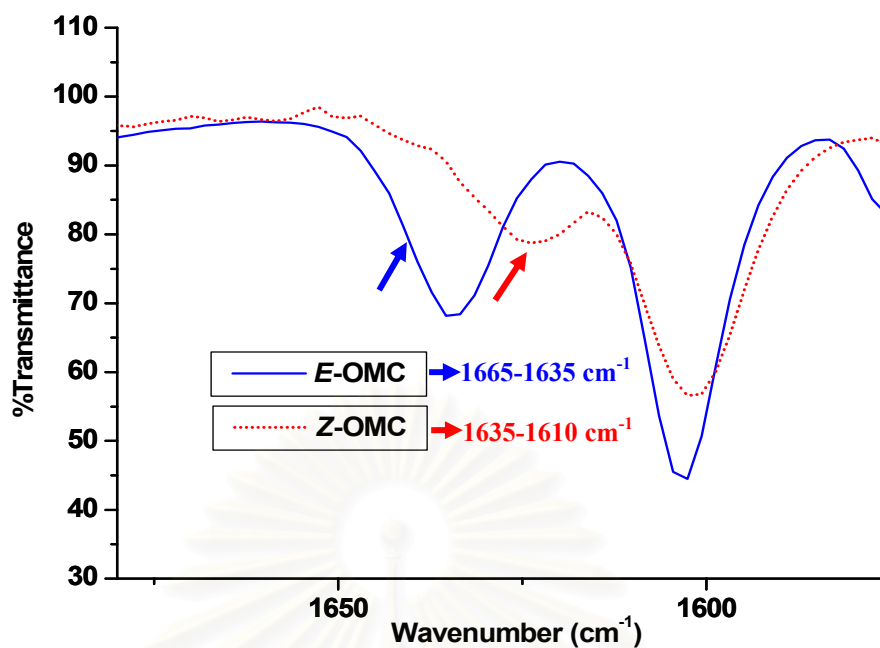


Figure 3.5 Expansion of the ATR-FTIR spectra of the *E*- and the *Z*-OMC in the 1665-1610 cm⁻¹ range.

In addition to the spectral difference between the *E*- and *Z*-configuration at 1665-1610 cm⁻¹, the CH out of plane deformation of the -CH=CH moiety at 720-690 cm⁻¹ present only for the *Z* configuration was demonstrated in Figure 3.6.

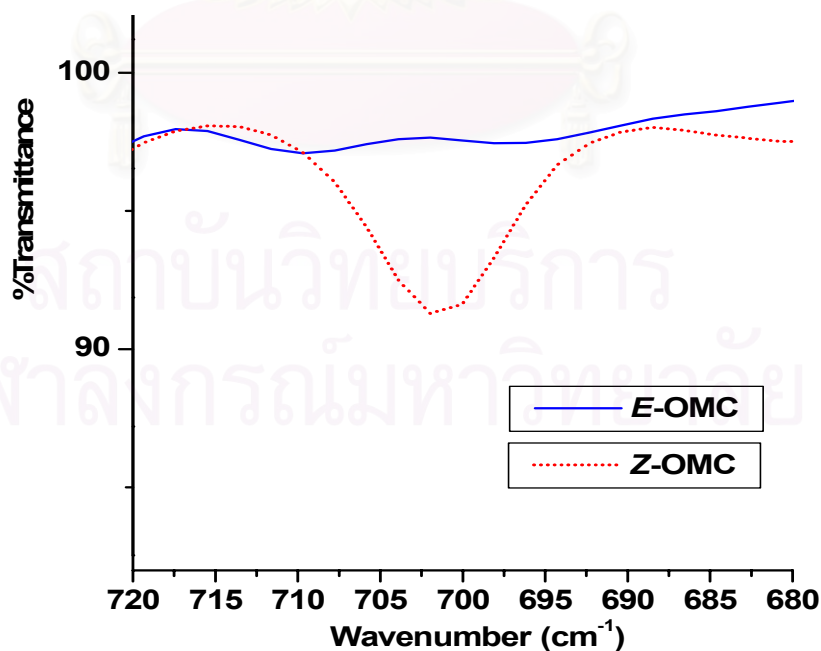


Figure 3.6 The differences of spectral intensities between the *E*- and *Z*-isomer in the frequency range of 720-680 cm⁻¹.

Another big difference between the *E*- and the *Z*-OMC IR spectrum stands at 981 cm^{-1} which corresponds to $-\text{CH}=\text{CH}-$ rocking deformation vibration detected only in the *E*- configuration. Figure 3.7 shows the IR-spectra of the *E*- and the *Z*-OMC at $1100\text{-}900\text{ cm}^{-1}$. It is very obvious that only *E*-OMC exhibits IR-peak at 981 cm^{-1} . This peak was used for monitoring the configuration change of OMC molecule in this work. Our experiments (binary phase calibration experiments discussed in p.30) also confirmed that the decrease in $[E\text{-OMC}] / [Z\text{-OMC}]$ corresponded to the decrease in ratio of [area of peak **b**] / [area of peak **a**].

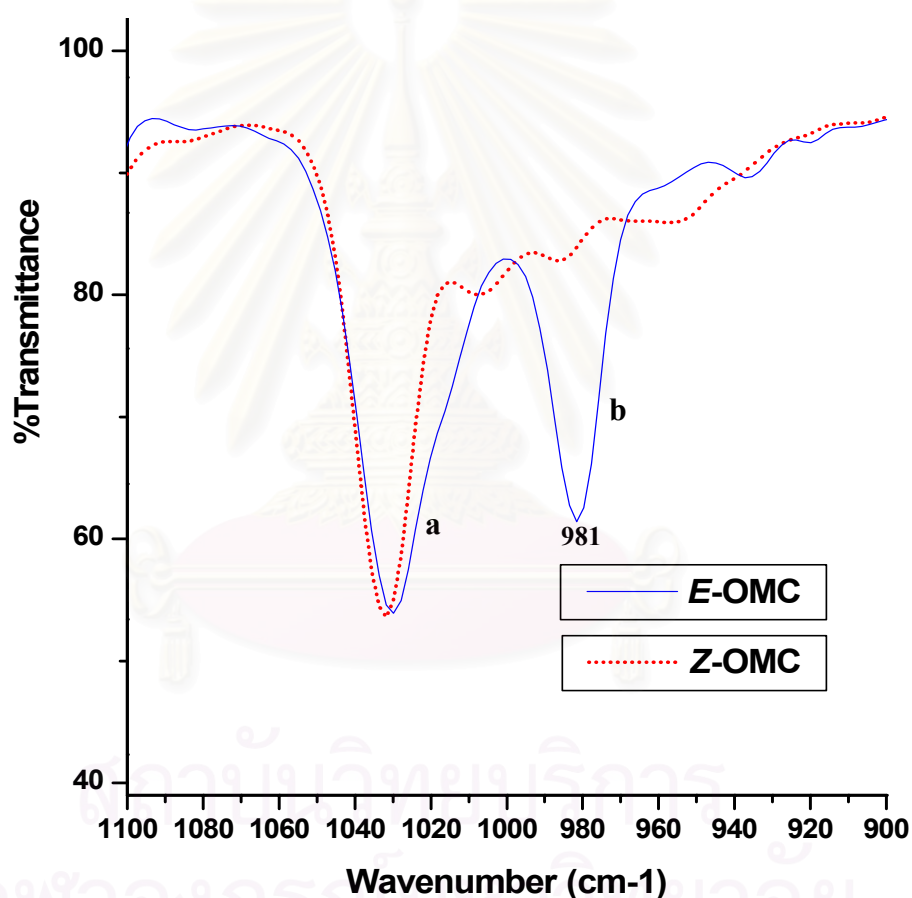


Figure 3.7 The differences of spectral intensities between the *E*- and *Z*-isomer in the frequency range of $998\text{-}964\text{ cm}^{-1}$.

3.2 Binary-phase calibration standards

Figure 3.8 shows a series of IR spectra of *E-Z* mixtures of different mole percents of the two configurations. It can be seen clearly that the **b** peak (981 cm^{-1}) intensity varies with $[E\text{-OMC}]/ [Z\text{-OMC}]$. In other words, intensity of the **b** peak increases as the amount of Z-OMC in the mixture decreases. To investigate the potential of using this ATR-FT-IR technique to quantify the *E*- and Z-OMC, several calibration standards containing 0, 10, 25, 50, 75, 90, and 100 mole percent of Z-isomer in the mixtures of *E*- and Z-OMC were constructed.

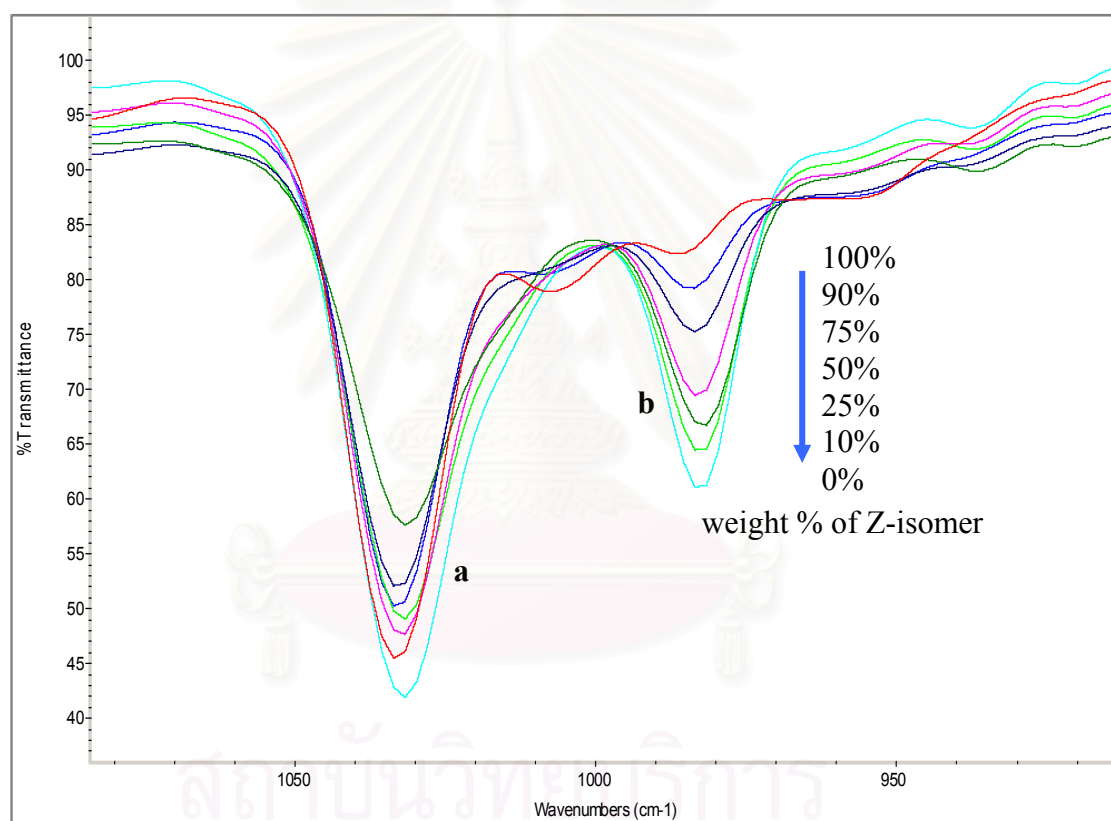


Figure 3.8 Overlaid ATR-FT-IR transmittance spectra of *E-Z* mixtures containing 0, 10, 25, 50, 75, 90, and 100 mole percent of Z-isomer in the mixtures of *E*- and Z-OMC. Total coverage of OMC (*E*-OMC + Z-OMC) was 1.34×10^{-7} moles/ cm^2 .

By plotting the ratio of peak area at 998-964 cm^{-1} (**b** peak; indicating *E*-configuration) and peaks at 1060-998 cm^{-1} (internal standard peak; **a** peak) which later will be called **b/a** ratio, against the mole percent of *Z*-isomer in the *E-Z* mixture, a linear calibration plot was obtained with a correlation coefficient (R^2) of 0.9872. A good linear relationship between mole percent of the *Z*-configuration and the **b** peak area could be obtained as demonstrated in Figure 3.9. In conclusion, by using the ratio of peak area at 998-964 cm^{-1} and 1060-998 cm^{-1} , mole percent of each configuration in the mixture of the two configurations could be determined

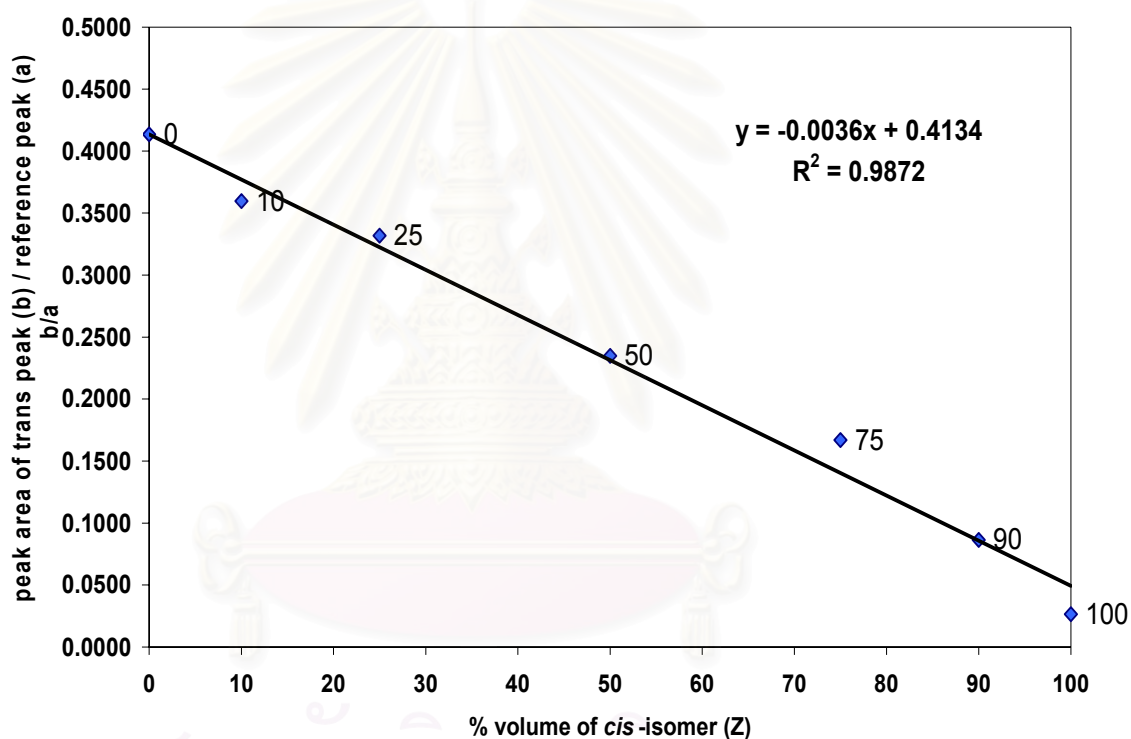


Figure 3.9 Calibration plot between b/a and mole percent of *Z*-OMC from ATR-FTIR taken of the binary -phase mixtures

3.3 Kinetic study of *E* to *Z* Photoisomerization on ZnSe

Figure 3.10 and 3.11 show the time-dependent spectral data for a single experiment when *E*-OMC was exposed to UVB light. The changes in 998-964 cm^{-1} peak intensities clearly indicated the *E* to *Z* configurational change on ZnSe surface when *E*-OMC was irradiated with UVB light. From the Figure, one can see that there was no change for the peaks at 2780-3100 cm^{-1} , therefore, the peaks can also be used as internal standard peak. This unchanged peaks at 2780-3100 cm^{-1} also indicated the reproducibility of our IR sampling procedure during each irradiation cycle.

The spectral sets of all coverages indicate similar results in which the *E*-OMC peak at 981 cm^{-1} (the **b** peak) decreases after being exposed to UVB light.

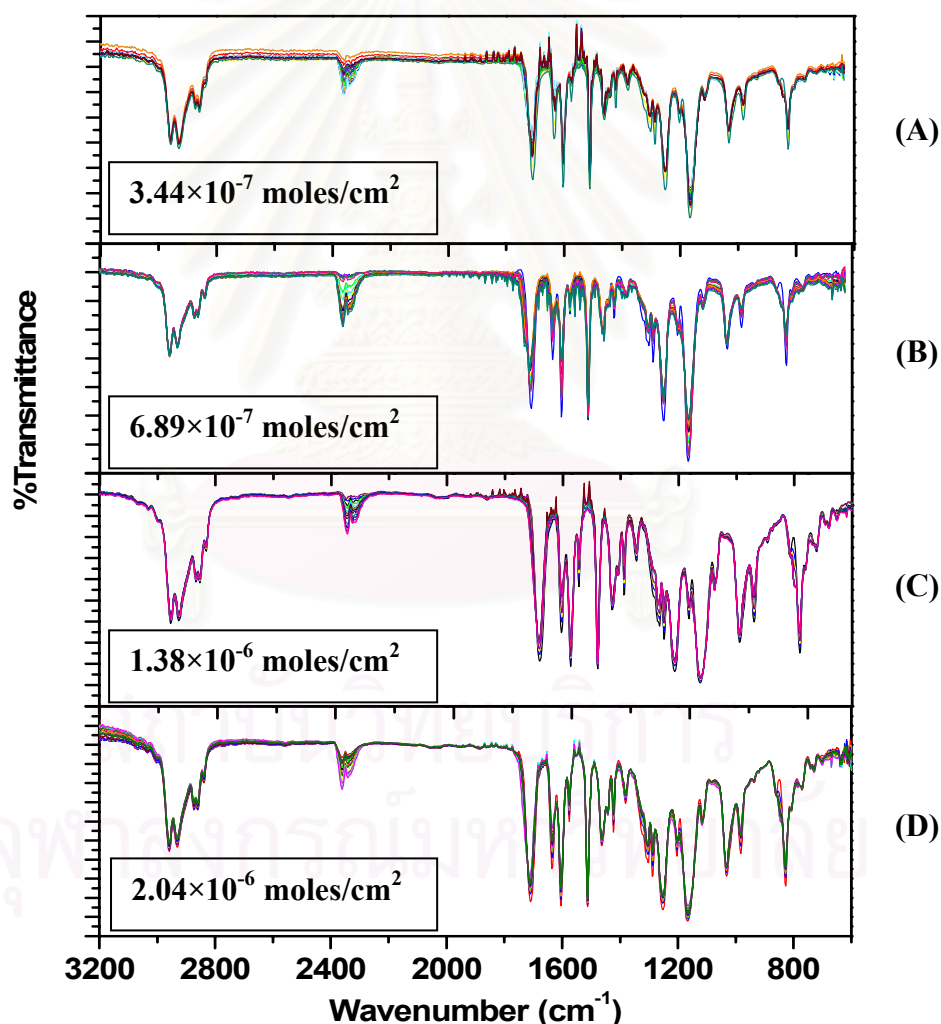


Figure 3.10 ATR-FTIR spectra showing photoisomerization of *E*-OMC on ZnSe at various times of exposure. Coverages of OMC on ZnSe were 3.44×10^{-7} moles/ cm^2 (A), 6.89×10^{-7} moles/ cm^2 (B), 1.38×10^{-6} moles/ cm^2 (C) and 2.04×10^{-6} moles/ cm^2 (D), respectively.

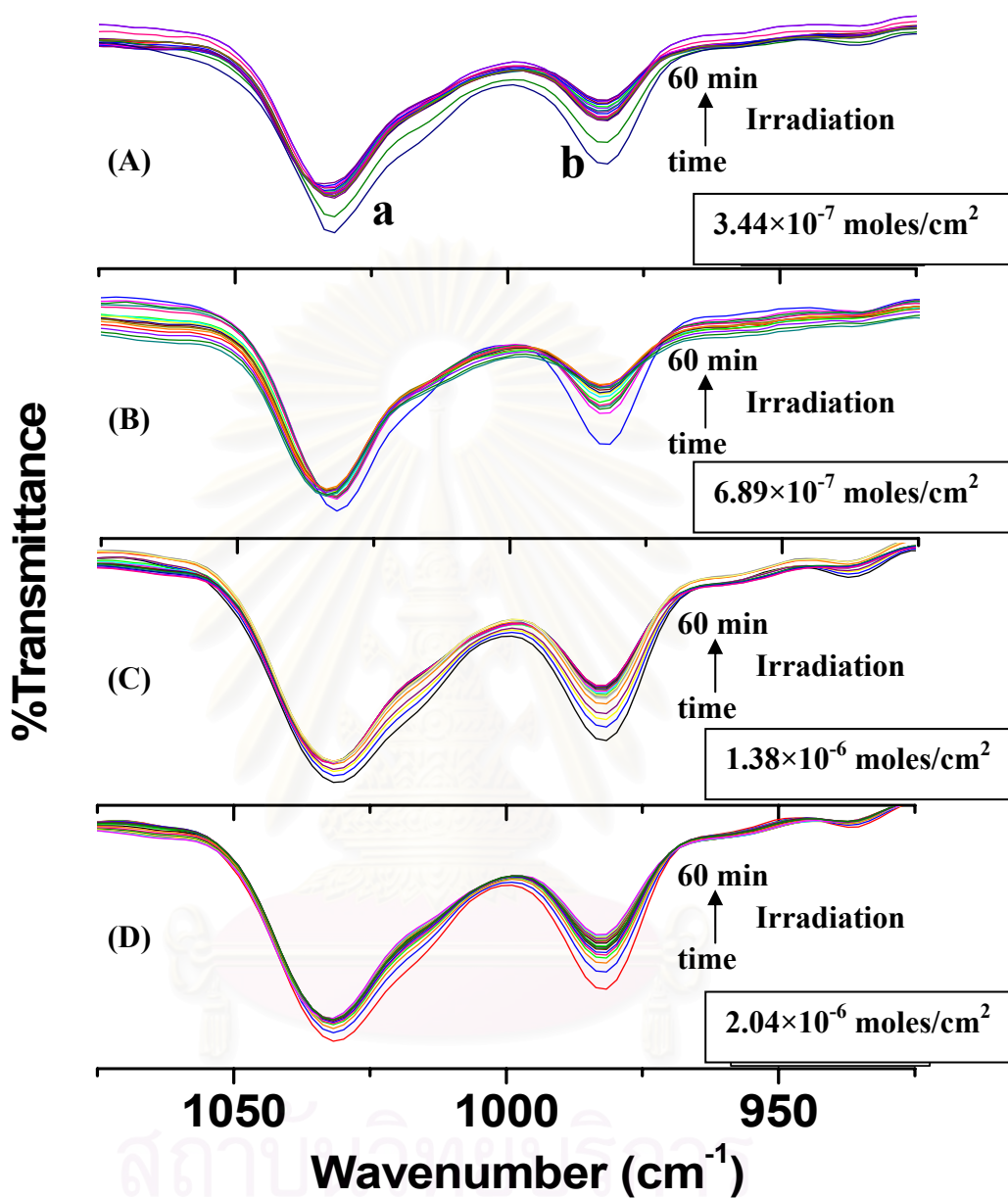


Figure 3.11 ATR-FTIR spectra showing photoisomerization of *E*-OMC on ZnSe at various times of exposure. These spectra are the expansions of the spectra in Figure 3.10.

As shown earlier that linear relationship between the **b/a** peak area ratio and the mole percent of Z-OMC has been elucidated, therefore from the information of **b/a** ratio mole percent of Z-OMC in the mixture could be obtained. Figure 3.12 shows the plot between the **b/a** peak area ratio against the UVB exposure time. Figure 3.13 then shows the plot between calculated mole percent of the Z-OMC and the UVB exposure time.

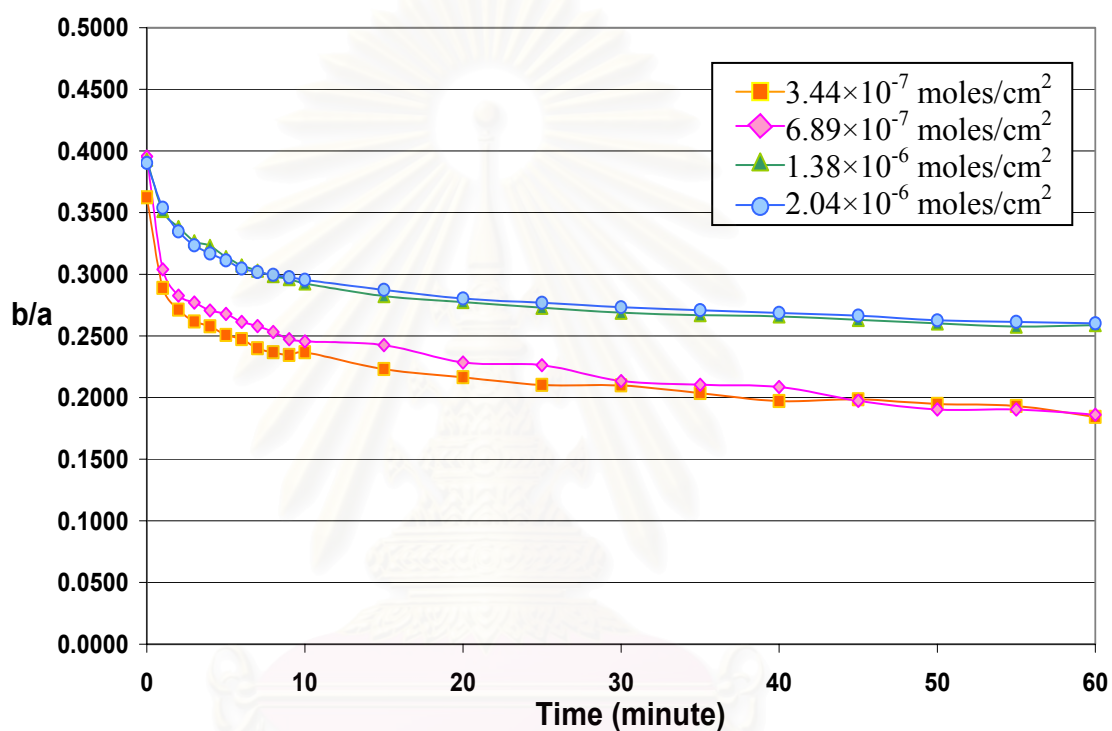


Figure 3.12 Plot of the peak area ratios **b/a** as a function of UVB exposure time from the *E* to *Z* experiment on ZnSe for (■) 3.44×10^{-7} moles/cm²; (◆) 6.89×10^{-7} moles/cm²; (▲) 1.38×10^{-6} moles/cm²; (●) 2.04×10^{-6} moles/cm² OMC coverage.

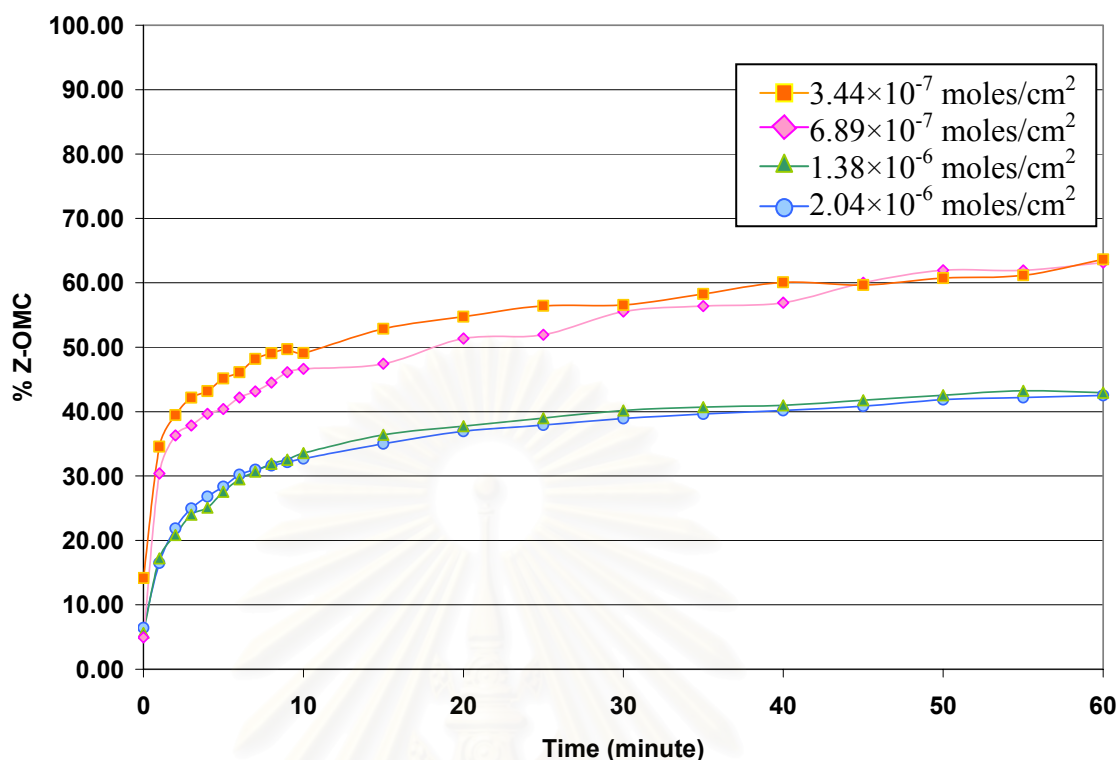


Figure 3.13 Plot of the mole percent of the Z-OMC as a function of UVB exposure time from the *E* to *Z* experiment on ZnSe for (■) 3.44×10^{-7} moles/cm²; (◆) 6.89×10^{-7} moles/cm²; (▲) 1.38×10^{-6} moles/cm²; (●) 2.04×10^{-6} moles/cm² OMC coverage.

It can be seen clearly that upon UVB exposure, *E*-OMC rapidly isomerized to the *Z*-configuration and the rate of isomerization then decreased. Photostationary equilibrium between the *E*- and the *Z*-OMC depended on the total coverage of OMC. Lower coverage gave higher *Z*-OMC at the photostationary equilibrium. This study was the first to show the configurational change of OMC on surface. The result, however, agreed with works done in solution in which more *Z*-OMC was also detected at photostationary equilibrium in solution of lower OMC concentration. (22)

It should be noted here that photostationary equilibrium usually will also depend on light intensity. In this experiment, the UVB intensity was 0.08 mW/cm^2 .

At much higher coverage of OMC on surface, much less configurational change was detected. This can be seen in Figure 3.14 and 3.15.

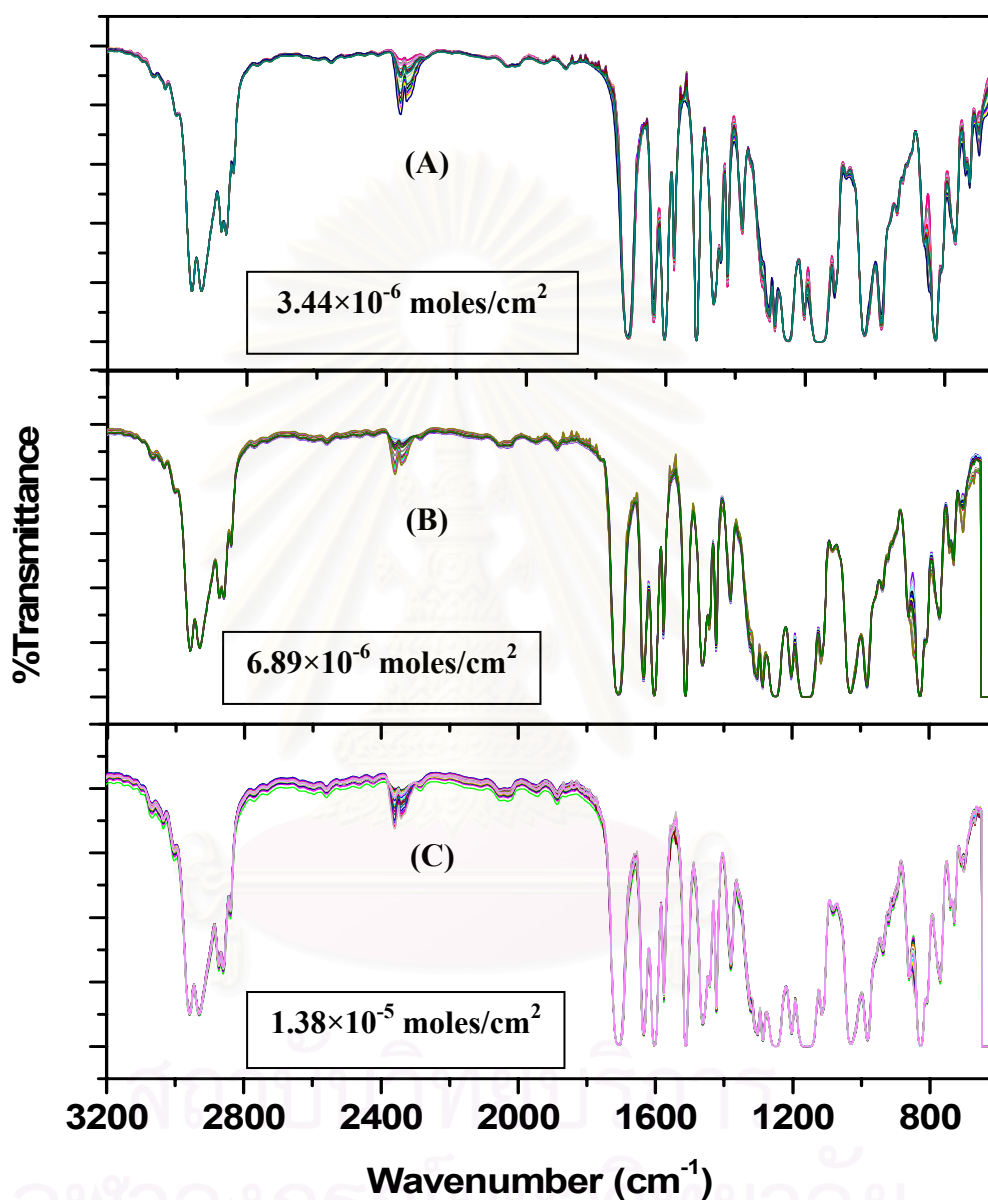


Figure 3.14 ATR-FTIR spectra showing photoisomerization of *E*-OMC on ZnSe at various times of exposure. Coverages of OMC on ZnSe were 3.44×10^{-6} moles/cm² (A), 6.89×10^{-6} moles/cm² (B) and 1.38×10^{-5} moles/cm² (C), respectively.

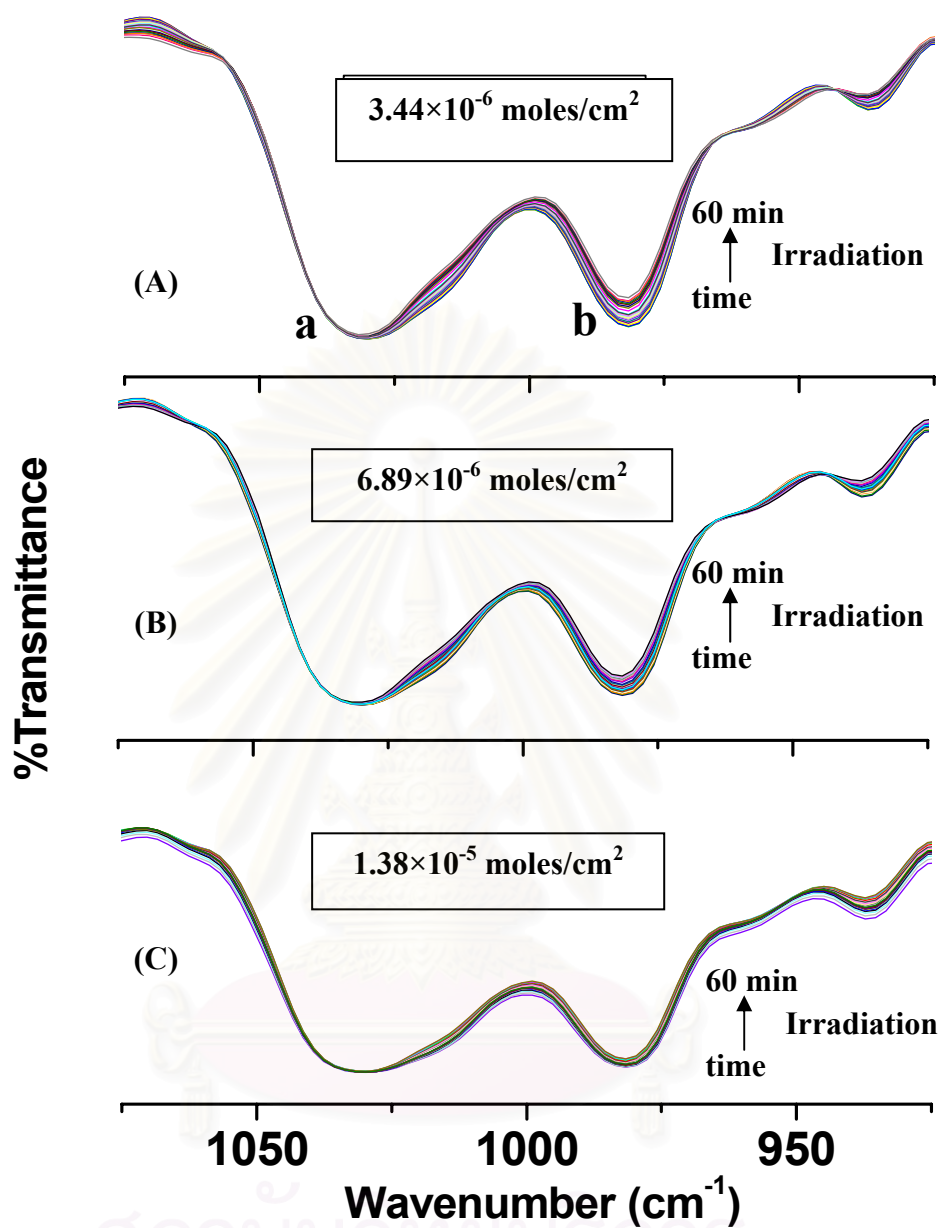


Figure 3.15 ATR-FTIR spectra showing photoisomerization of *E*-OMC on ZnSe at various times of exposure. These spectra are the expansions of the spectra in Figure 3.14.

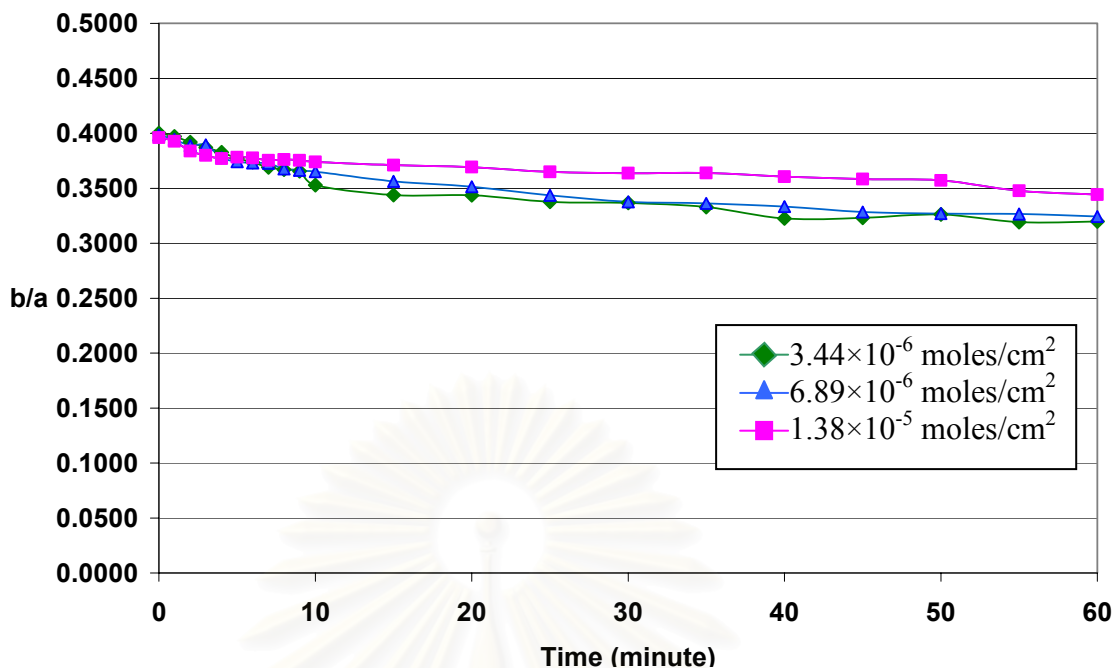


Figure 3.16 Plot of the peak area ratios b/a as a function of UVB exposure time from the E to Z experiment for (◆) 3.44×10^{-6} moles/cm²; (▲) 6.89×10^{-6} moles/cm²; (■) 1.38×10^{-5} moles/cm² of OMC on ZnSe.

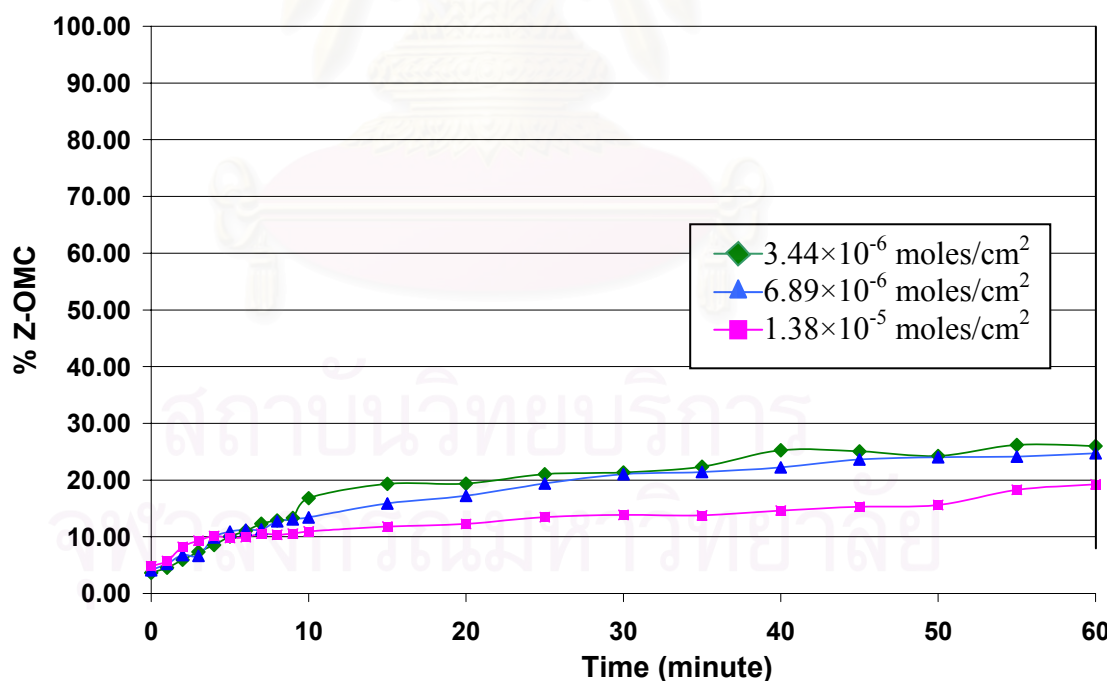


Figure 3.17 Plot of the mole percent of the Z-OMC as a function of UVB exposure time from the E to Z experiment for (◆) 3.44×10^{-6} moles/cm²; (▲) 6.89×10^{-6} moles/cm²; (■) 1.38×10^{-5} moles/cm² of OMC on ZnSe.

From Figure 3.16-3.17, it can be concluded that at UVB irradiance of 0.08 mW/cm^2 , almost no *E* to *Z* configurational change was observed when OMC coverage reached $1.38 \times 10^{-5} \text{ moles/cm}^2$. Since the recommended coverage of OMC on skin surface is around 2 mg/cm^2 or $6.89 \times 10^{-6} \text{ mole/cm}^2$, small *E* to *Z* configurational changes may occur during the molecules are on the skin. However, the UVB intensity in the sunlight also varies among different location and time, therefore, degree of *E* to *Z* photoisomerization will also depend on location and time too. Figure 3.18 shown the plot of UVB intensities in Bangkok measured during the clear sky day. The 0.08 mW/cm^2 intensity chosen in this study falls into the UVB irradiance around noon time in Bangkok.

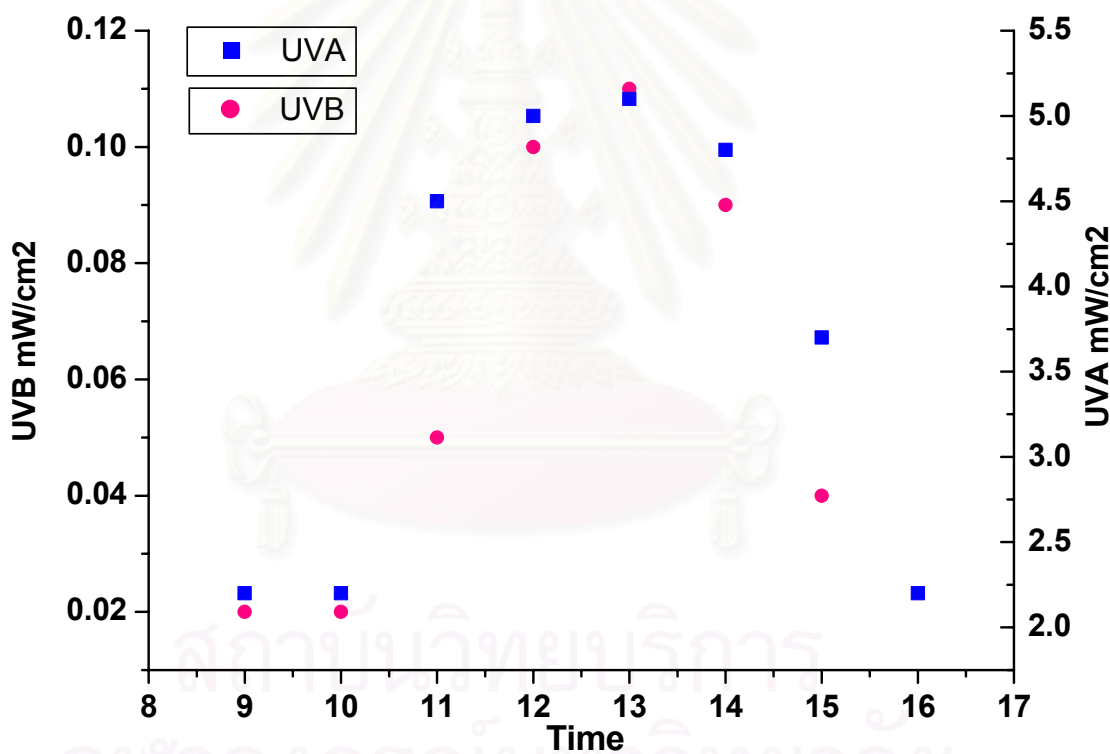


Figure 3.18 Plot of UVB intensities in Bangkok measured during the day.

3.4 Kinetic study of *E to Z* Photoisomerization on rat skin

Figure 3.19 shows spectral results for the kinetic analyses of OMC on rat skin. Spectra were collected at 0-60 minutes of UVB exposure time.

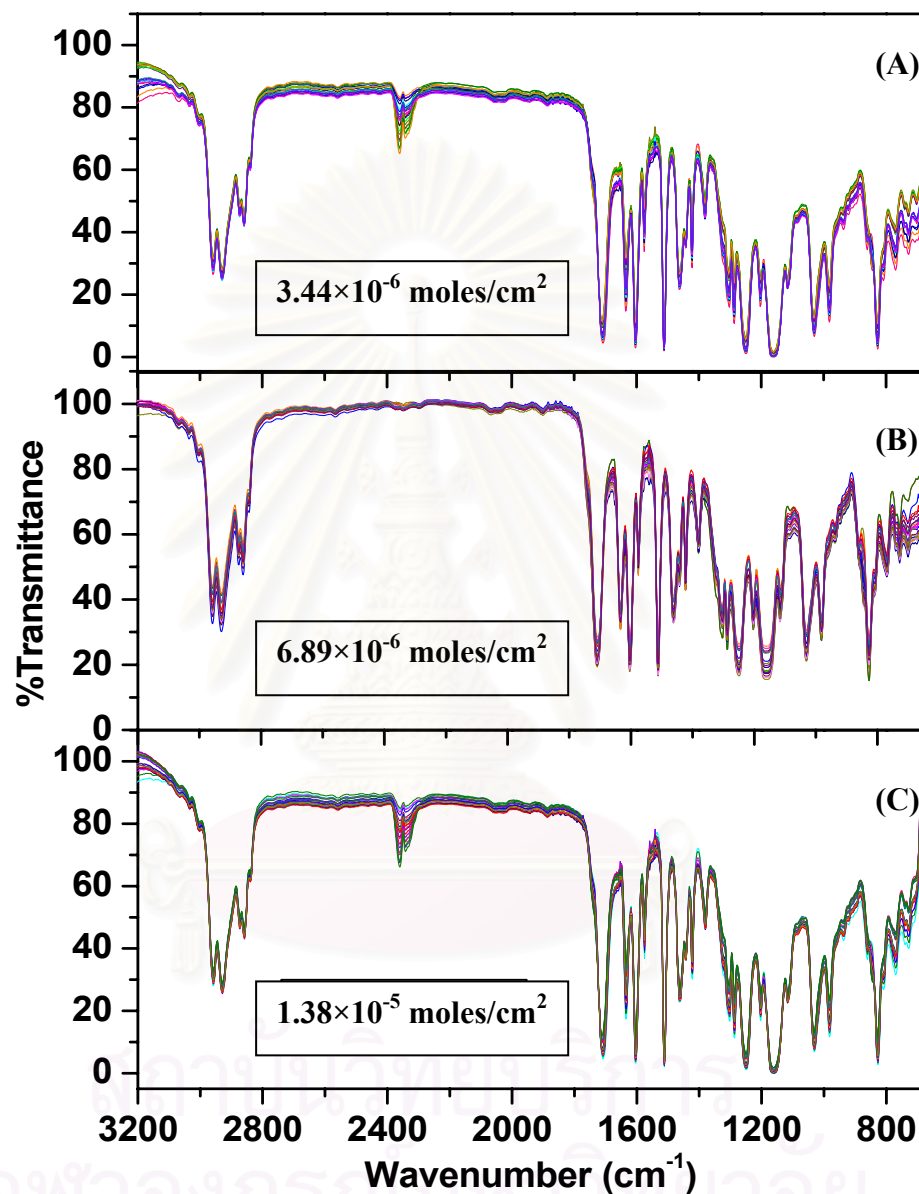


Figure 3.19 ATR-FTIR spectra showing photoisomerization of *E*-OMC on rat skin at various times of exposure. Coverages of OMC on rat skin were 3.44×10^{-6} moles/cm² (A), 6.89×10^{-6} moles/cm² (B) and 1.38×10^{-5} moles/cm² (C), respectively.

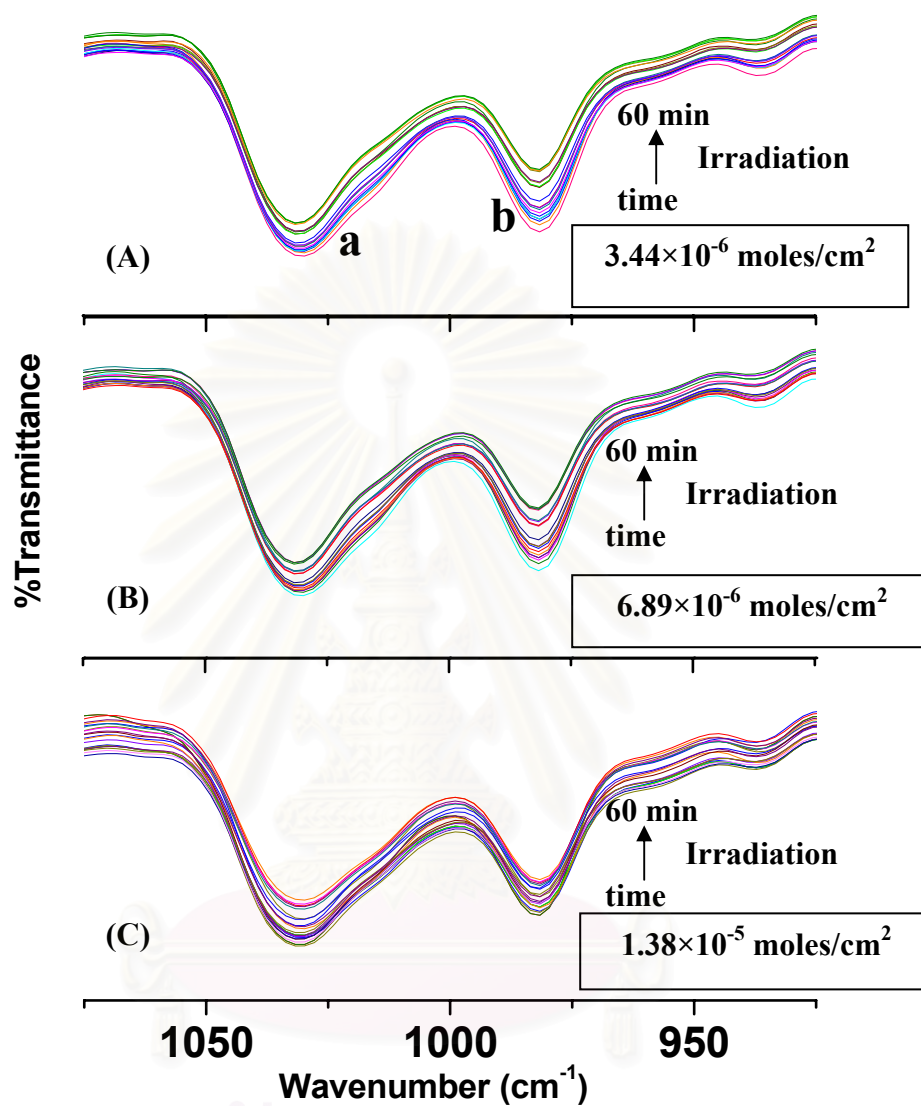


Figure 3.20 ATR-FTIR spectra showing photoisomerization of *E*-OMC on rat skin at various times of exposure. These spectra are the expansions of the spectra in Figure 3.19.

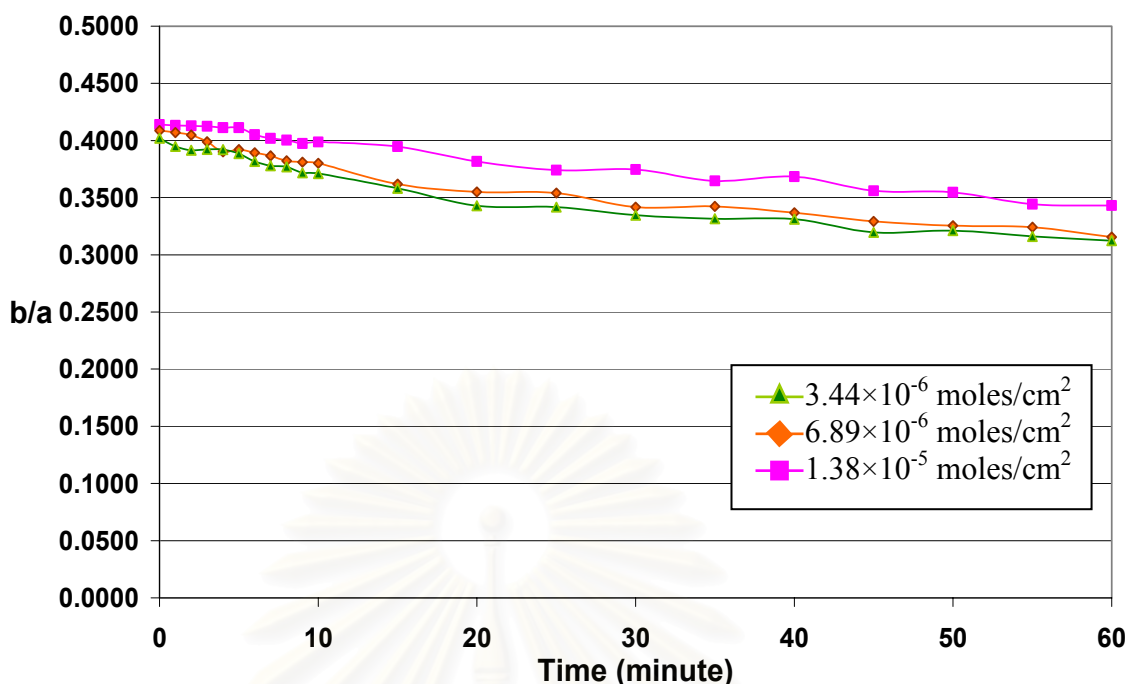


Figure 3.21 Plot of the peak area ratios b/a as a function of UVB exposure time from the E to Z experiment for (▲) 3.44×10^{-6} moles/cm²; (◆) 6.89×10^{-6} moles/cm²; (■) 1.38×10^{-5} moles/cm² of OMC on rat skin.

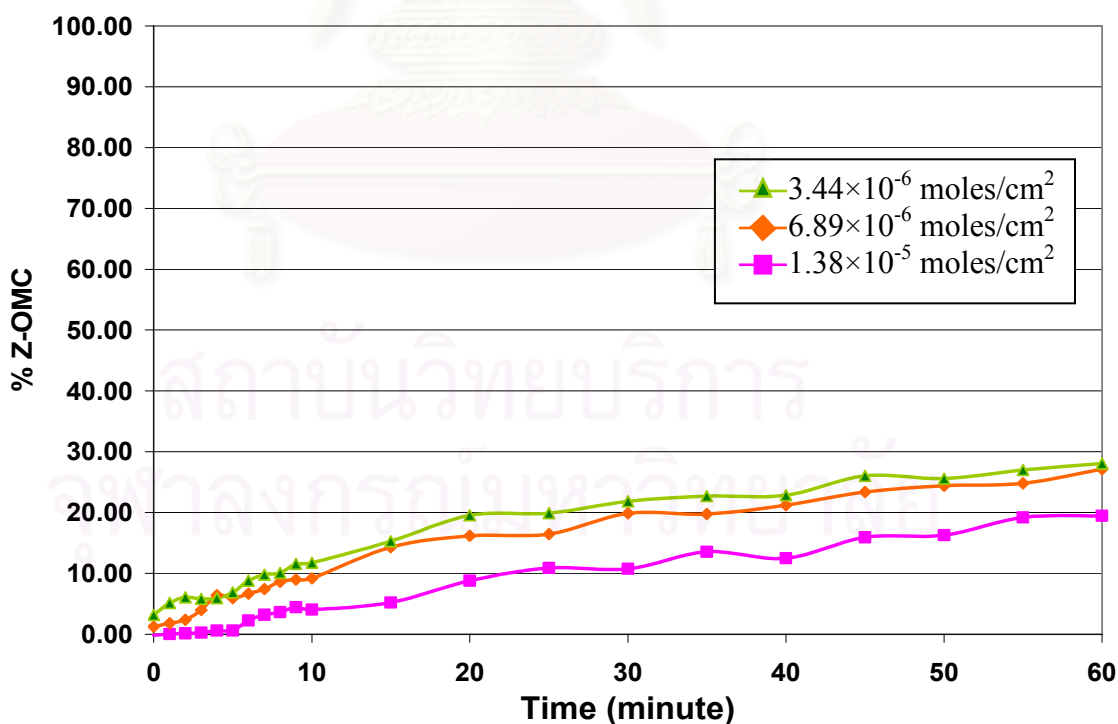


Figure 3.22 Plot of the mole percent of the Z-OMC as a function of UVB exposure time from the E to Z experiment for (▲) 3.44×10^{-6} moles/cm²; (◆) 6.89×10^{-6} moles/cm²; (■) 1.38×10^{-5} moles/cm² of OMC on rat skin.

As can be seen in Figure 3.20-3.22, the trend of photoisomerization of *E*- to *Z*-OMC on rat skin was similarly to that on ZnSe surface (see Figure 3.23).

However, higher degree of *E*- to *Z*-configurational change could be seen on rat skin comparing to on ZnSe surface. This may due to the fact that there were some water molecules in the rat skin. The polarity of water molecule may aid the change in configuration upon returning to ground state of the twisted-excited state. (22) This result again agrees with previous works which indicated that more *E* to *Z* configurational change of OMC could be found in more polar solvent.

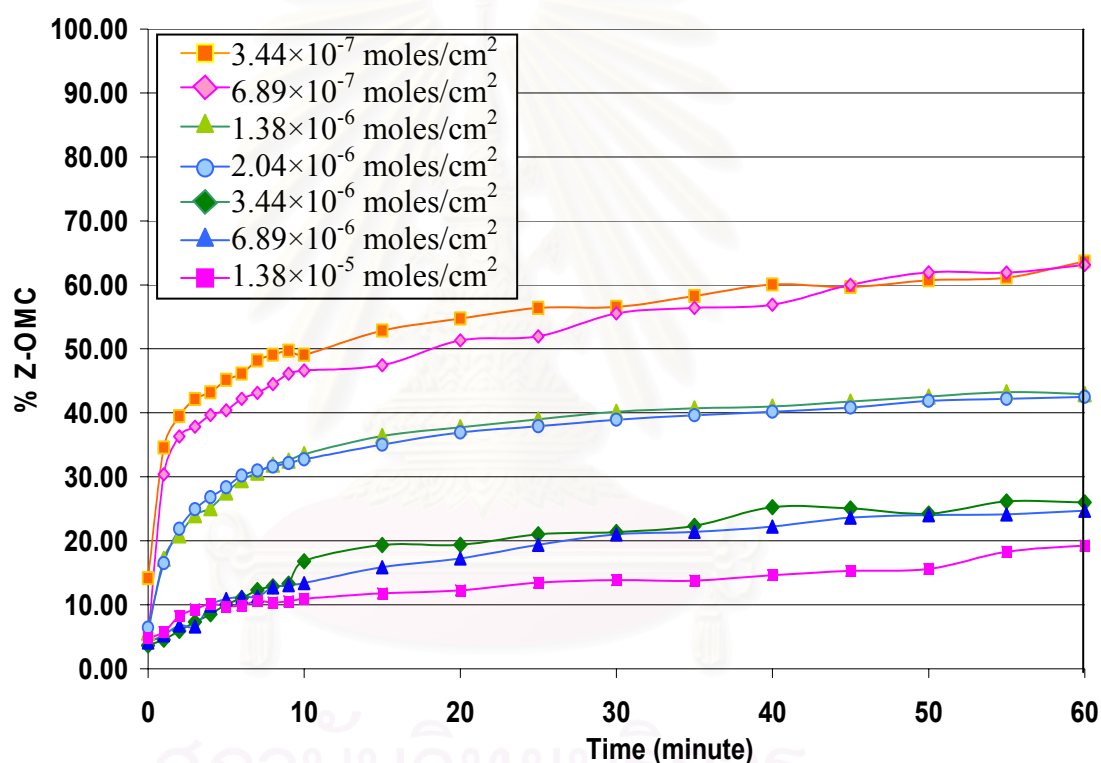


Figure 3.23 Plot of the mole percent of the *Z*-OMC as a function of UVB exposure time from the *E* to *Z* experiment for (■) 3.44×10^{-7} moles/cm²; (◇) 6.89×10^{-7} moles/cm²; (▲) 1.38×10^{-6} moles/cm²; (●) 2.04×10^{-6} moles/cm²; (◆) 3.44×10^{-6} moles/cm²; (▲) 6.89×10^{-6} moles/cm² and (■) 1.38×10^{-5} moles/cm² of OMC on ZnSe.

3.5 Kinetic study of *Z* to *E* Photoisomerization on ZnSe

When *Z*-OMC, which was separated from the mixture of *E*- and *Z*-OMC by column chromatography, was applied on ZnSe and analyzed by ATR-FTIR technique to monitor *Z* to *E*-photoisomerization, configurational change from *Z* to *E* was detected.

A b band (964-998 cm^{-1}) could be detected in spectrum of *Z*-OMC after UV exposure (see Figure 3.24). The intensity of this band, which was assigned to *trans* >CH=CH< group, reached the maximum after about 30 minute and then remained approximately constant. This corresponded to the net change from *Z* configuration to *E* configuration before the photostationary equilibrium was reached. The situation was similar to the *E* to *Z* photoisomerization described earlier.

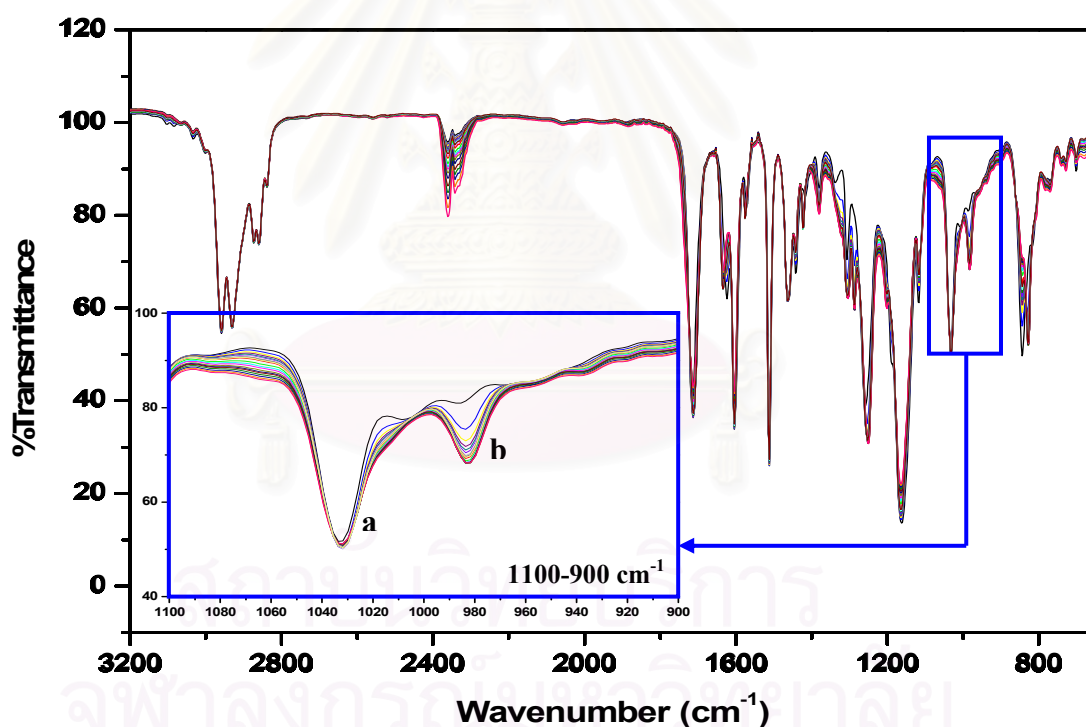


Figure 3.24 ATR-FTIR spectra showing photoisomerization of *Z*-OMC on ZnSe at various times of UVB exposure. Coverage of OMC on ZnSe was 1.34×10^{-7} moles/cm².

The work on rat skin implies that at the recommended coverage of OMC on skin, UVB protection efficiency will decrease as the skin is exposed to UVB light. This is rationalized from the previous study which indicated that Z-OMC possesses the molar absorption coefficient value of about $12,000 \text{ M}^{-1}\text{cm}^{-1}$ to the value of $24,000 \text{ M}^{-1}\text{cm}^{-1}$ for the E-OMC.²²

Moreover, since more comparing E to Z configurational change occurs at lower OMC coverage, this implies that skin with lower coverage of OMC not only has less protection at the beginning but also will lose protection upon UV exposure to a greater extent comparing to skin with higher coverage of OMC.

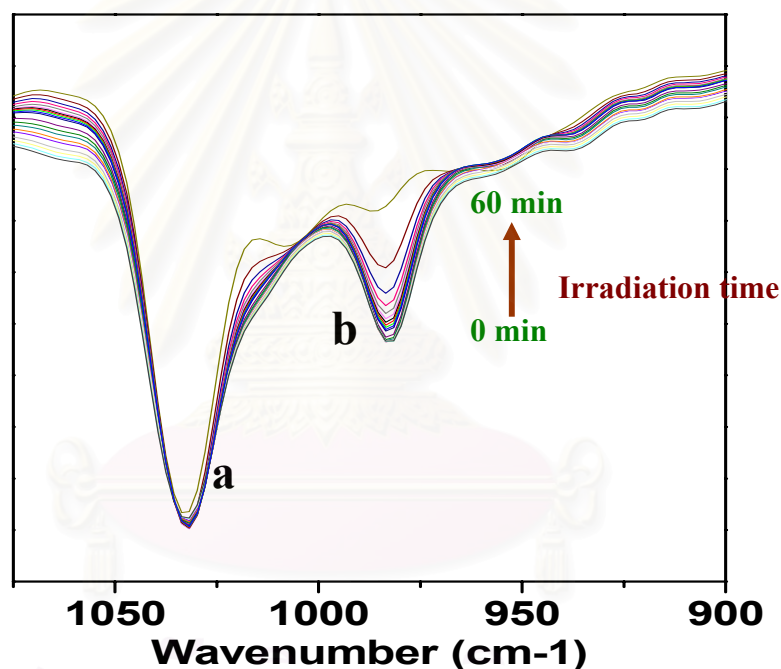


Figure 3.25 Expansion of the ATR-FTIR spectra in the $1100\text{-}900 \text{ cm}^{-1}$ range showing photoisomerization of Z-OMC on ZnSe after various UVB exposure times (between 0-60 min).

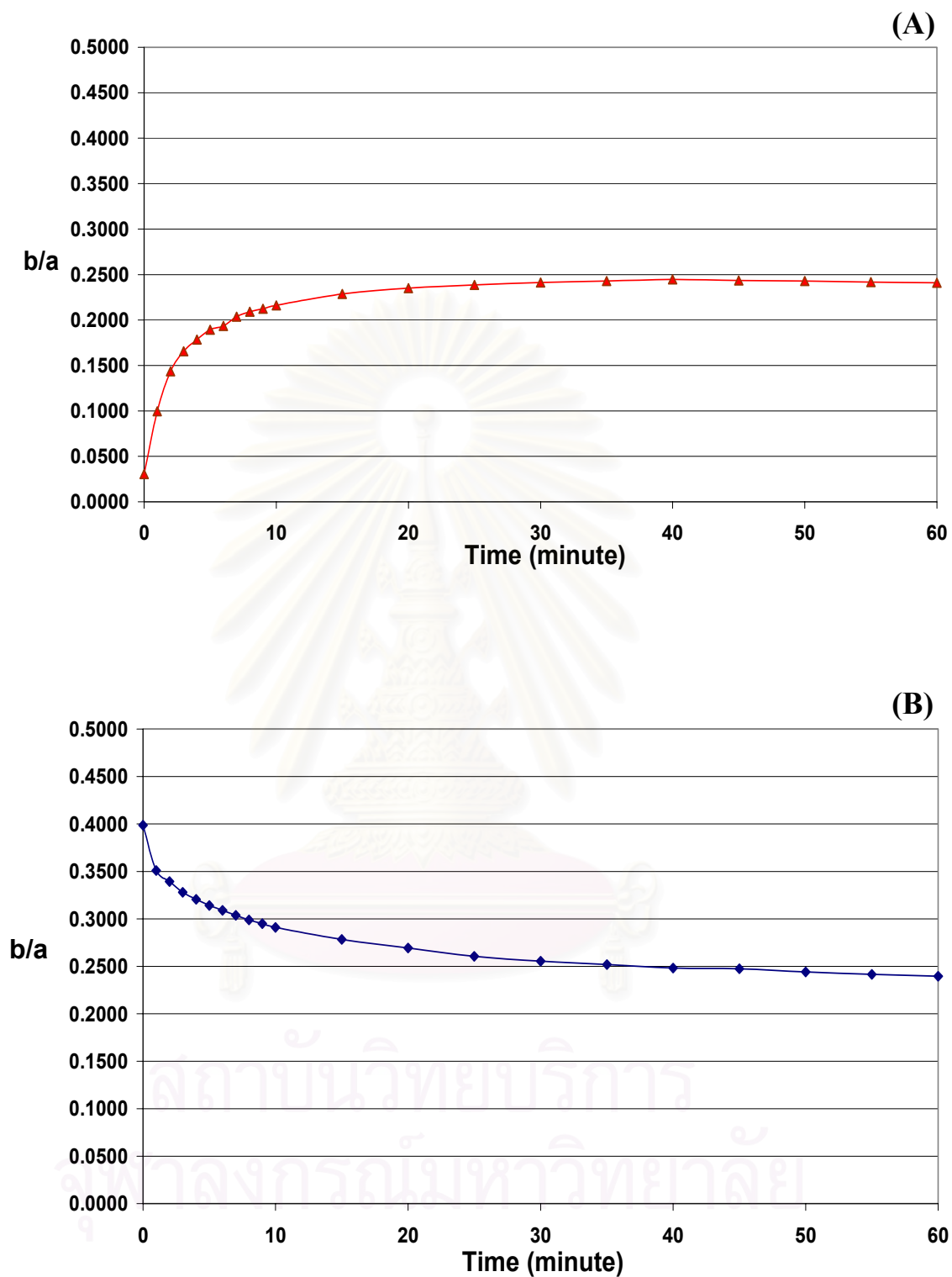


Figure 3.26 Plots of the peak area ratios b/i as a function of UVB exposure times for 1.34×10^{-7} moles/cm² of OMC on ZnSe. (A) Z- to E-photoisomerization; (B) E- to Z-photoisomerization.

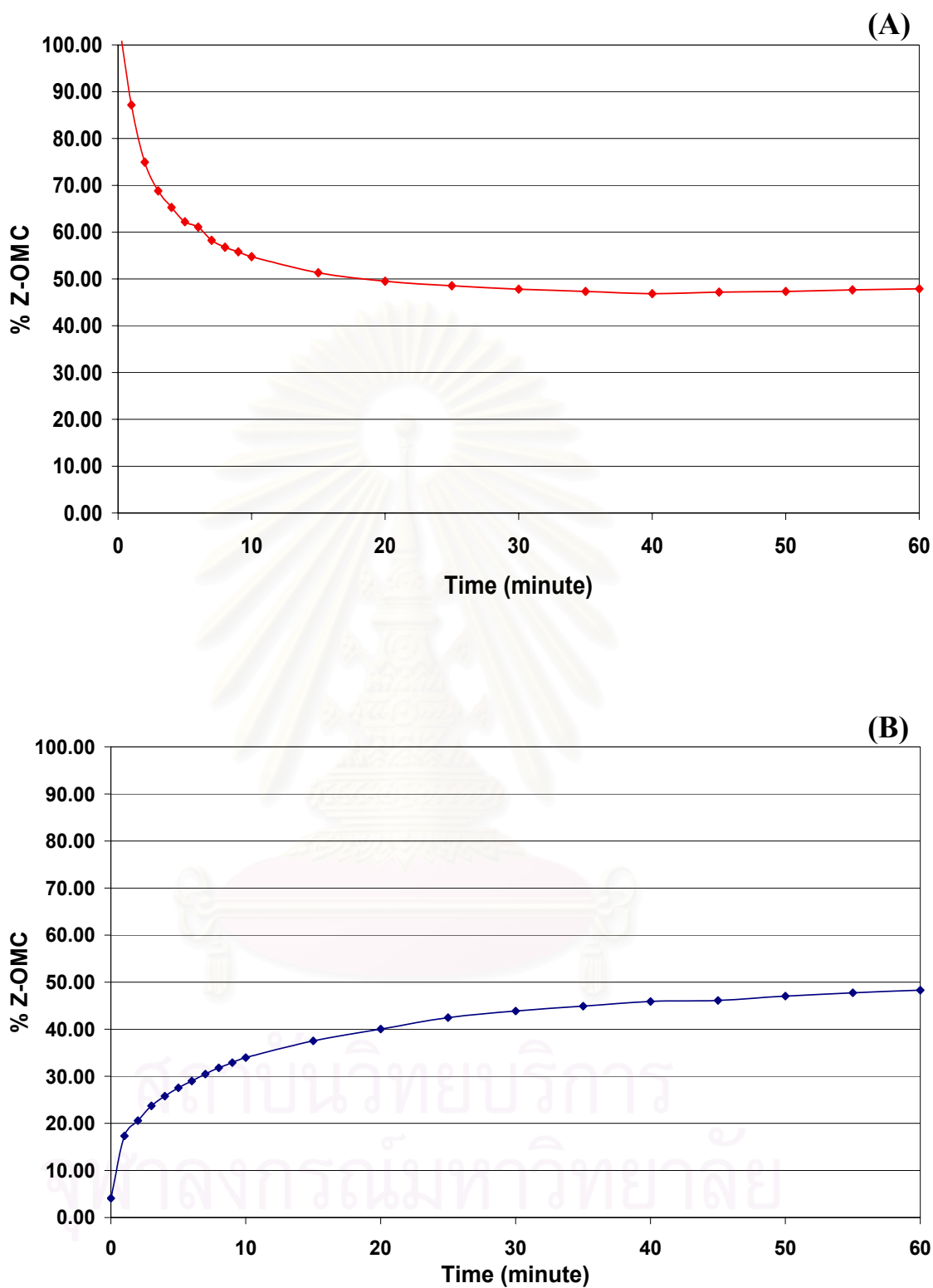


Figure 3.27 Plots of the mole percent of the Z-OMC as a function of UVB exposure time for 1.34×10^{-7} moles/cm² of OMC on ZnSe for (A) Z to E photoisomerization, (B) E to Z photoisomerization.

As demonstrated in Figure 3.27, at OMC coverage of 1.34×10^{-7} moles/cm² of OMC on ZnSe, with UVB lamp at 0.08 mW/cm², both the *E* and the *Z* configuration eventually reached the same photostationary equilibrium where the ratio of *E*:*Z* was 1:1. However, the *Z* configuration took less time (~20 min) than the *E* configuration (~30 min) to reach the photostationary equilibrium.



สถาบันวิทยบริการ
จุฬาลงกรณ์มหาวิทยาลัย

CHAPTER IV

CONCLUSION

In this work we have demonstrated the *E* to *Z* configurational change of the commonly used UVB filter, octyl methoxycinnamate on ZnSe and rat skin surface upon the UV irradiation. Photoisomerization of both *E*- to *Z*-OMC and *Z*- to *E*-OMC was monitored through ATR-FTIR spectroscopy. The results indicated that photostationary equilibrium was affected by amount of OMC coverage and more configurational changes were observed at lower coverage of OMC. Photoisomerization on ZnSe and rat skin showed only small differences in which a little more isomerization was detected on rat skin surface comparing to the ZnSe surface. At the recommended use of OMC coverage on skin which is about 2 mg/cm², and at the UVB irradiance of 0.08 mW/cm² (corresponds to UVB in sunlight around noon time in Bangkok on clear sky day), configurational change from *E*- to *Z*-OMC was observed and the *E*:*Z* ratio at the photostationary equilibrium was about 3:1. This work has, therefore, implied that upon UVB exposure, small decrease in UVB absorption efficiency of OMC will be induced. This results from the fact that *Z*-OMC has only about half absorption coefficient value comparing to that of the *E*-OMC (~24,000 M⁻¹cm⁻¹).

สถาบันวิทยบริการ
จุฬาลงกรณ์มหาวิทยาลัย

REFERENCES

1. Lowe, N. J., Shaath, N. A., and Pathak, M. A. *Sunscreen Development, Evaluation, and Regulatory Aspects*. 2nd ed. New York, USA: Marcel Dekker, **1997**, P.83-85, 268-280.
2. Forbes, P. D. "Relevance of animal models of photocarcinogenesis to humans" *Photochem. Photobiol.* **1996**, 63(4), 357-362.
3. Grant, William B. "An estimate of premature cancer mortality in the US due to inadequate doses of solar ultraviolet-B radiation" **2002**,
4. LeVee G.J., Oberhelman L., Anderson T., Koren H., and Cooper K.D. "UVA II exposure of human skin results in decreased immunization capacity, increased induction of tolerance and a unique pattern of epidermal antigen-presenting cell alteration" *Photochem Photobiol.* **1997**, 65, 622–629.
5. Lowe, N.J., and Shaath, N. A. "Sunscreen development, evaluation and regulatory aspects" Marcel Dekker: New York , **1990**, P.216-233.
6. Dransfield, G., Guest, P.J., Lyth, P.L., Mcgyrvey, D.J., and Truscott, T.G., "Photoactivity test of TiO₂-based inorganic sunscreens partI: Non-aqueous dispersions" *J. Photochem. Photobiol.* **2000**, 59, 147-151.
7. Hancock-chen, T., and Scaiano, J.C. "Enzyme inactivation by TiO₂ photosensitization" *J. Photochem. Photobiol.* **2000**, 57, 193-196
8. Wamer, Wayne G., Yin, J.J., and Wet, R.R. "Oxidative damage to nucleic acids photosensitized by titanium dioxide" *Free Rad. biol. med.*,**1997**, 23(6), 851-858.
9. Umbach, W. "Cosmetics and Toiletries Development, Production and Use" New York, USA: Midsomer Norton, Avon, Ellis Horwood Limited, **1991**, P.96.
10. Chisvert, A., Pascual-Marti, M.C., and Salvador, A. "Determination of UV-filters in sunscreens by HPLC" *Fresenius. J. Anal. Chem.* **2001**, 369, 638–641.
11. Jiang, R., Roberts, M.S., Prankerd, R.J., and Benson, H.A. "Percutaneous absorption of sunscreen agents from liquid paraffin: self-association of octyl salicylate and effects on skin flux" *J. Pharm. Sci.* **1997**, 86, 791–796.

12. Lu, Z., Bei, J., and Wang, S. "A method for the preparation of polymeric nanocapsules without stabilizer" *J. Control. Release.* **1999**, *61*, 107–112.
13. Gupta, V.K., Zatz, J.L., and Rerek, M., Percutaneous absorption of sunscreens through micro-yucatan pig skin in vitro. *Pharm. Res.* **1999**, *16*, 1602–1607.
14. Darvay, A., White, I. R., Rycroft, R. J. G., Jones, A. B., and Hawk, J. L. M. "Photoallergic contact dermatitis is uncommon" *J. Dermatol.* **2001**, *145*, 597-601.
15. Ricci, C., Pazzaglia, M., and Tosti, A. "Photocontact dermatitis from UV filters" *contact Dermatitis.* **1998**, *38*, 343-344.
16. Hayden, C. G. J., Roberts, M. S., and Benson, H. A. E. "Systemic absorption of sunscreen after topical application" *The lancet.* **1997**, *350*, 863-864.
17. Benech-Kieffer, F., Wegrich, P., Schwarzenbach, R., and Klecak, G. "Percutaneous absorption of sunscreens in vitro: Interspecies comparison, skin models and reproducibility aspects" *Skin Pharmacol. Appl. Skin Physiol.* **2000**, *13*, 324-335.
18. Shaath, N. A., Fares, H. M., and Klein, K. "Photodegradation of Sunscreen Chemicals" *Cosm. & Toil.* **1990**, *105*, 41-44.
19. Meijer, J., and Londen, M. "Stability Analysis of Three UV-Filters Using HPLC" *J. liq. Chromat.* **1995**, *18*, 1821-1832.
20. Tarras-wahlberg, N., Stenhagen, G., Larko, O., Rosen, A., Wennberg, A. M., and Wennerstrom, O. "Changes in Ultraviolet Absorption of Sunscreens After Ultraviolet Irradiation" *J. Invest. Dermatol.* **1999**, *113*, 547-553.
21. Pattanaargson, S., and Limphong, P. "Stability of Octyl methoxycinnamate and Identification of Its Photo-Degradation Product" *Int. J. Cosmet. Sci.* **2001**, *23*, 151-158.
22. Pattanaargson, S., Munhapol, T., Hirunsupachot, P. and Luangthongaram, P. "Photoisomerization of Octyl Methoxycinnamate" *J. photochem. Photobiol.* **2004**, *161*, 269-274.
23. Fahrenfort, J. "Attenuated Total Reflection a New Principle for the Production of Useful Infra-red Reflection Spectra of Organic Compounds". *Spectrochim. Acta.* **1961**, *17*, 698-709.

24. Harrick, N. J (Ed.). *Internal Reflection Spectroscopy*. New York, USA: Harrick Scientific Corporation, **1979**.
25. Chalmers, J. M., Griffiths, P.R. *Hand book of vibratory spectroscopy: Sampling Technique*. UK: John Wiley&sons, Inc., **2002**. 949-950.
26. Silverstein, R. M. and Webster. F. X. *Spectrometric Identification of Organic Compounds*. 6th ed. New York, USA: John Wiley&sons, Inc., **1997**.



สถาบันวิทยบริการ
จุฬาลงกรณ์มหาวิทยาลัย



APPENDICES

สถาบันวิทยบริการ
จุฬาลงกรณ์มหาวิทยาลัย

APPENDIX A

PICTURES OF INSTRUMENTS AND ACCESSORIES USED IN THE EXPERIMENT



Nicolet Magna-760 FTIR spectrometer



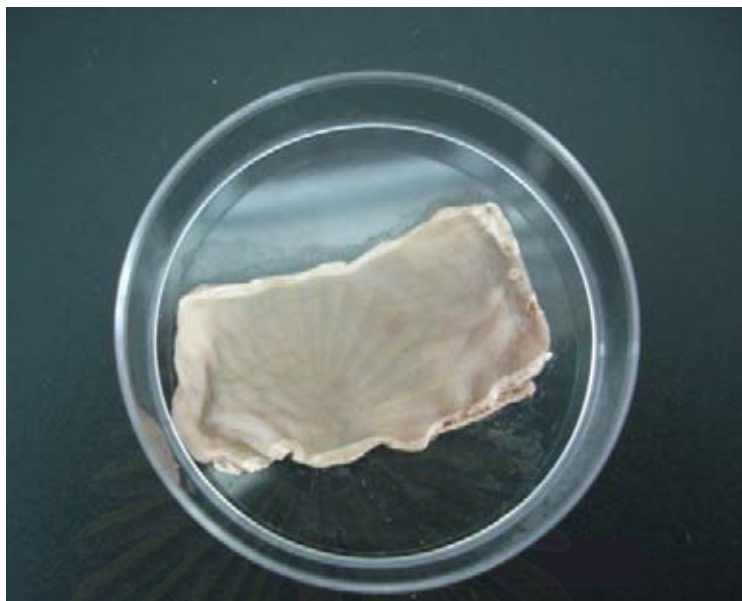
Multiple-reflection planar crystal (ZnSe) and accessories



Variable angle attachment accessory (The Seagull™)



Daavlin Psorawand UV lamp: PW-UVB-220



Skin specimens of 3 week olds mouse.



Skin specimen of rat after UVB irradiation at 0.08 mW/cm^2 for 60 min

APPENDIX B

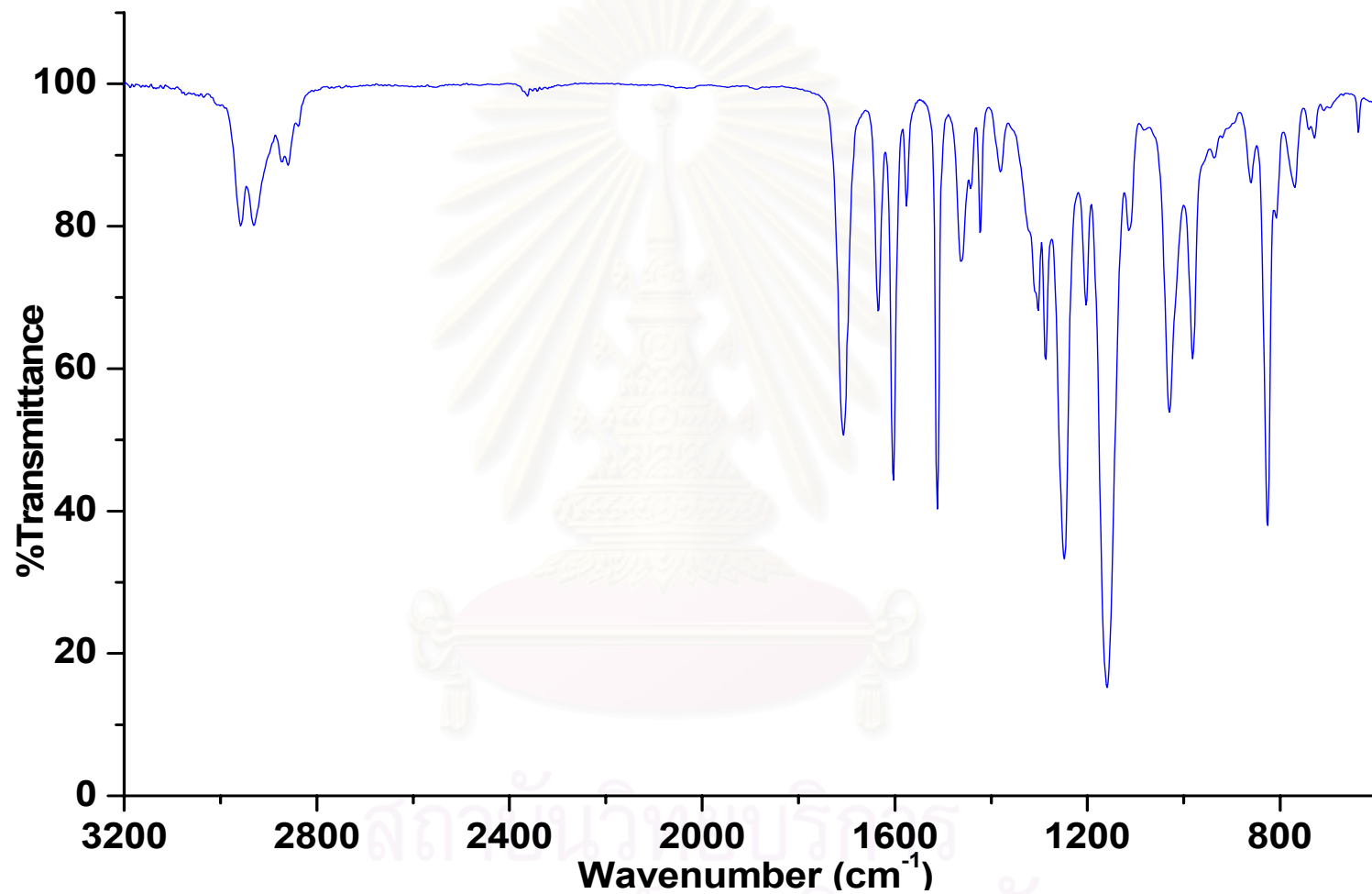


Figure B.1 IR spectrum of *E*-OMC

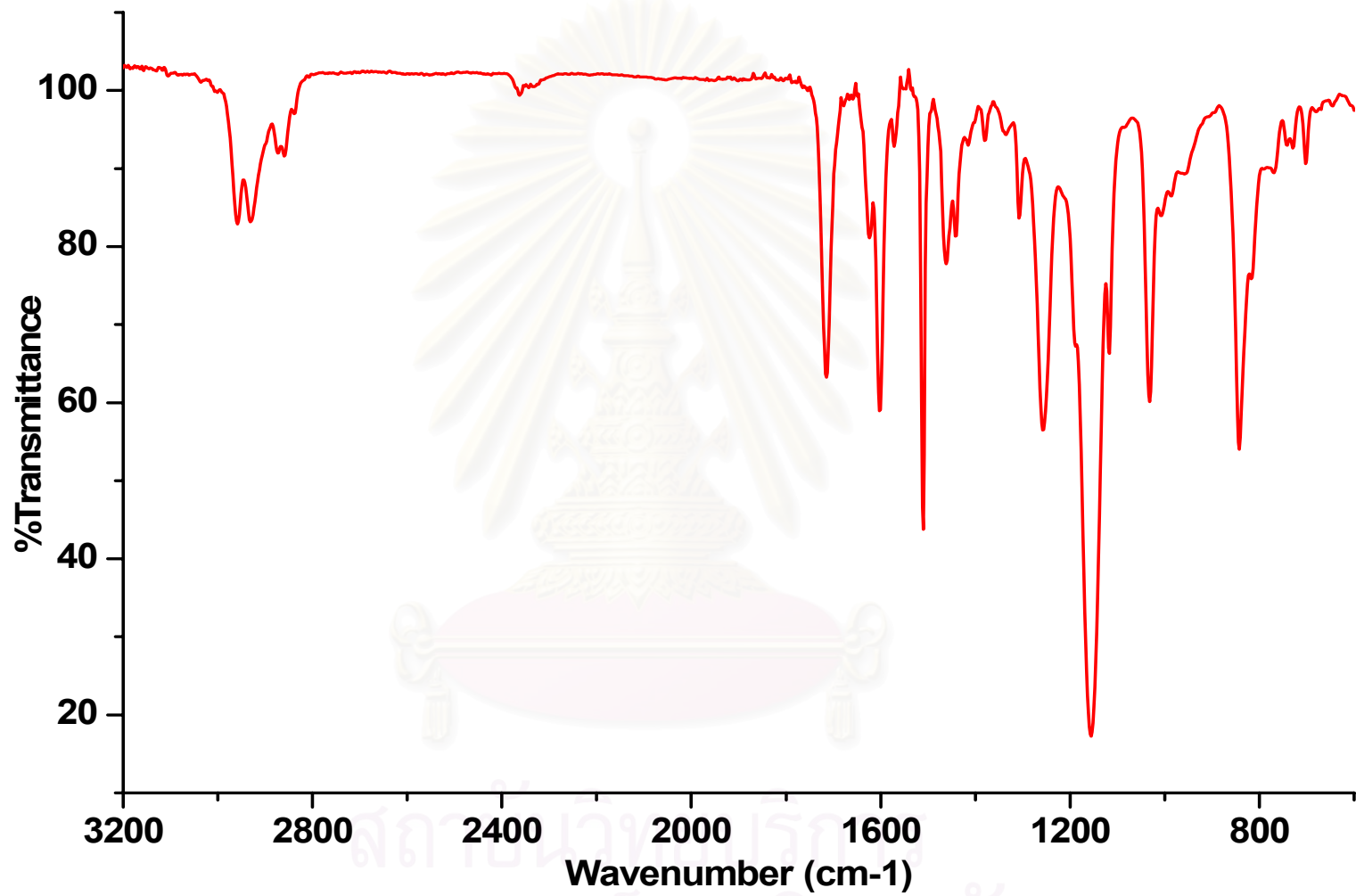


Figure B.2 IR spectrum of Z-OMC

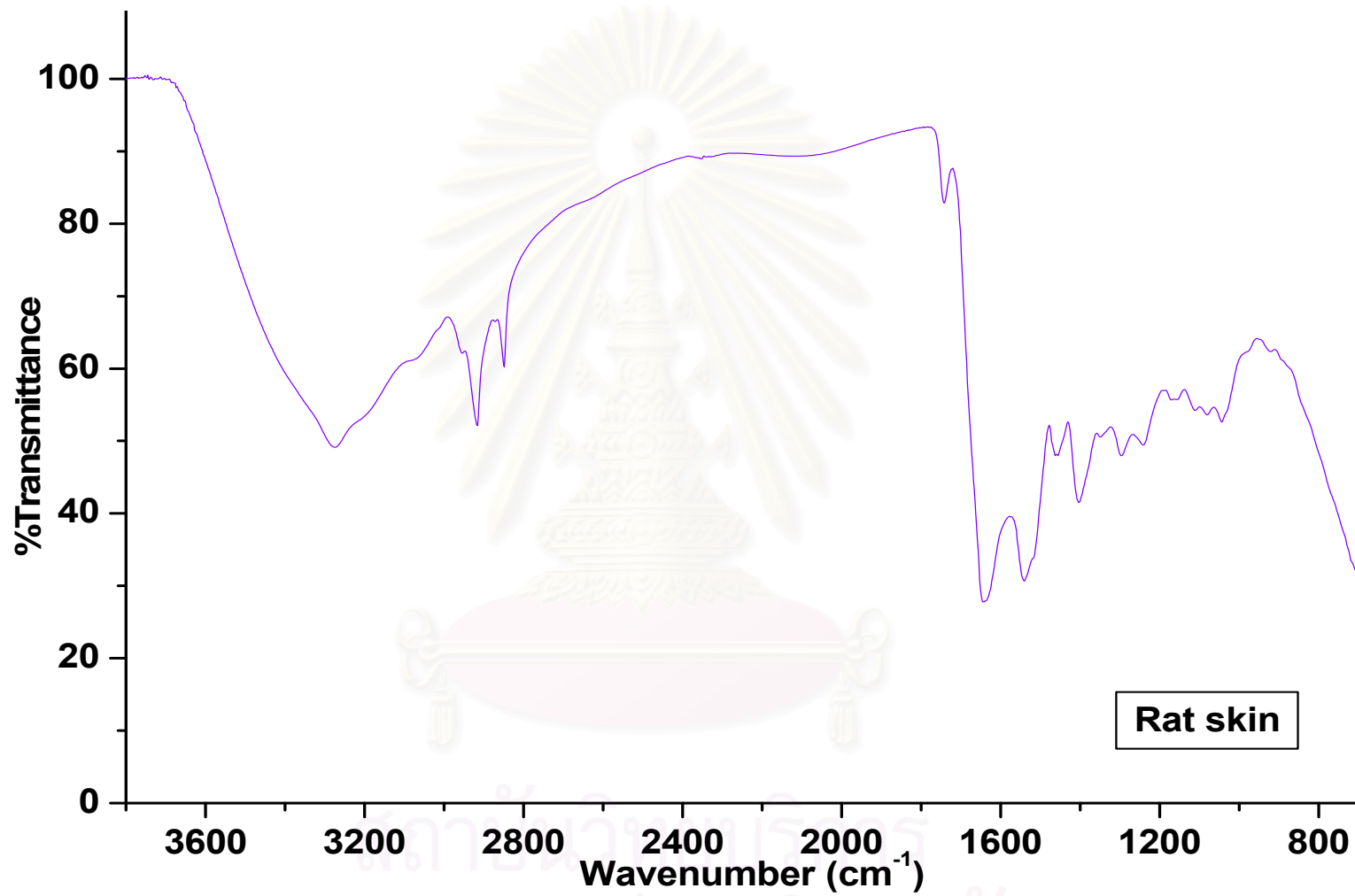


Figure B.3 IR spectrum of rat skin

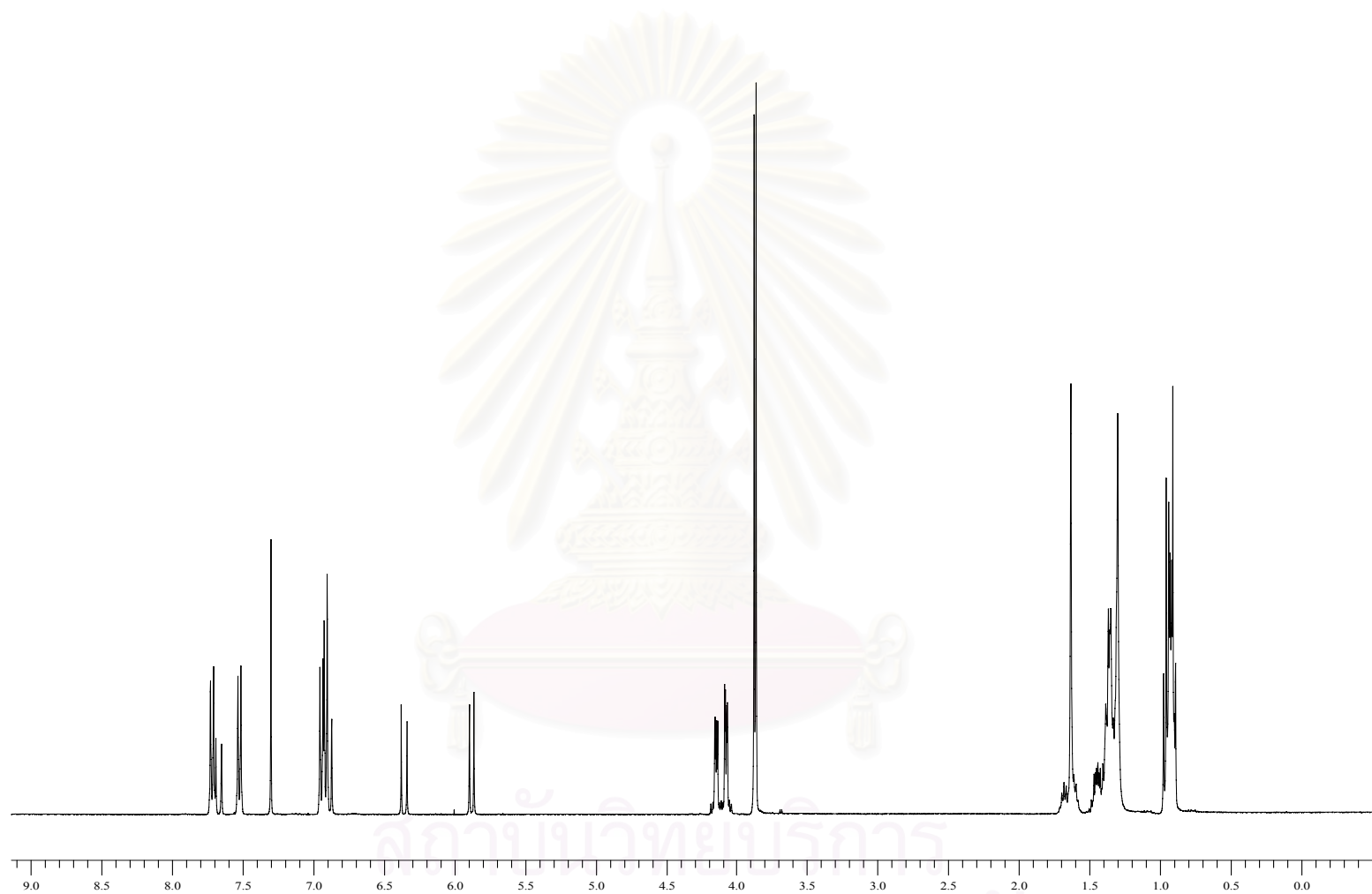


Figure B.4 ^1H NMR of mixture of *E*- and *Z*-OMC

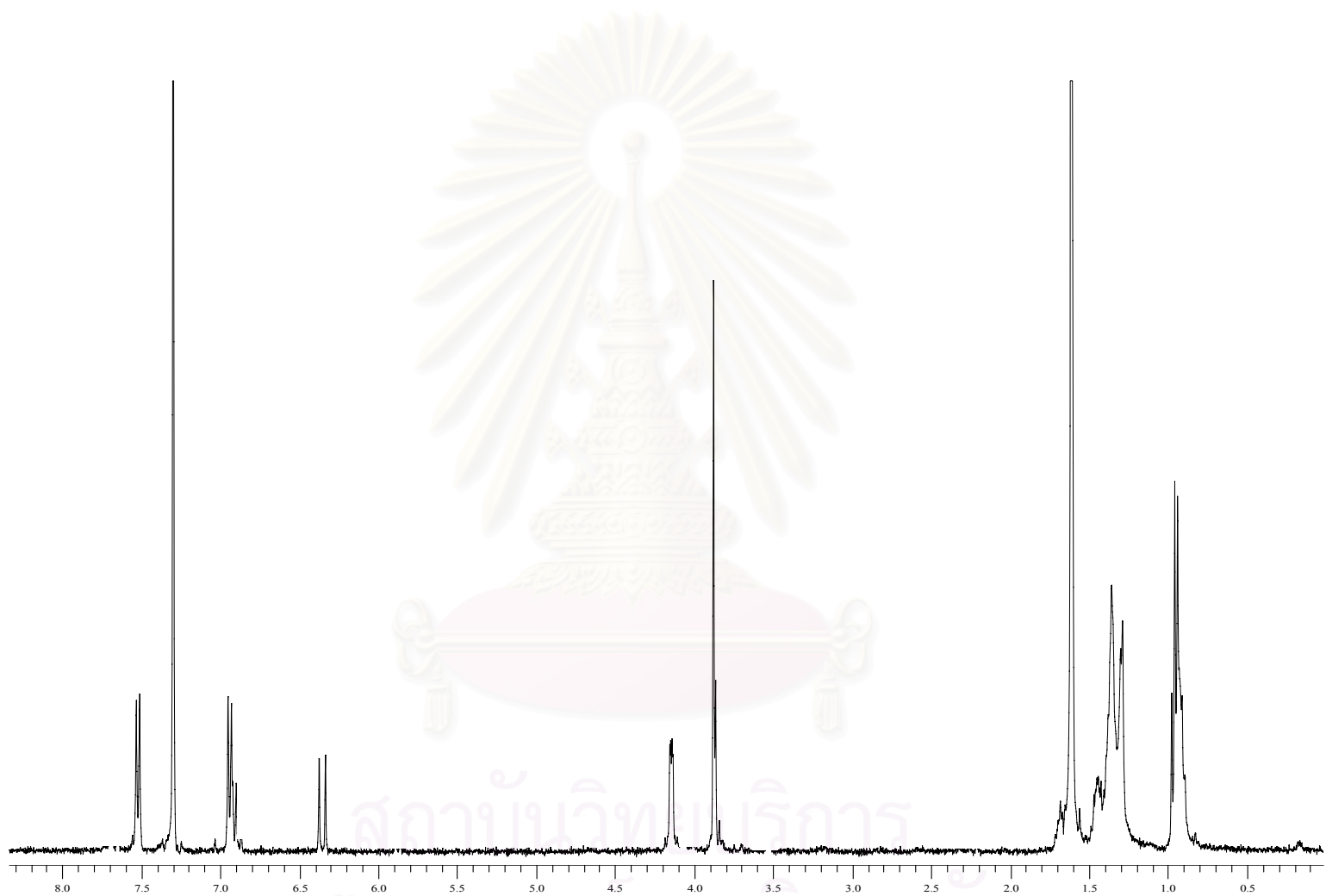


Figure B.5 ^1H NMR of *E*-OMC

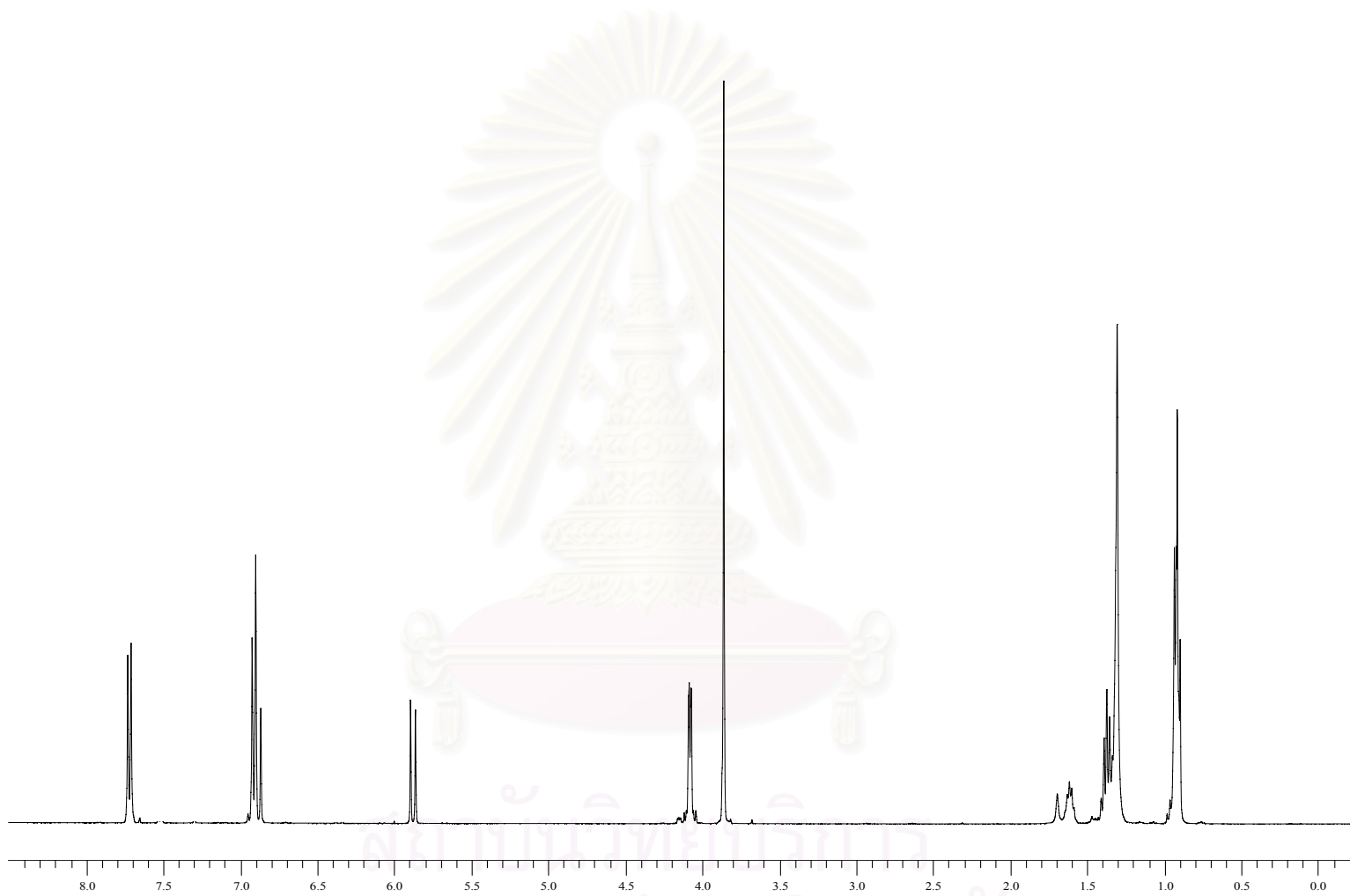


Figure B.6 ^1H NMR of Z-OMC

VITA

Miss Pattaraporn Pangnakorn was born on November 8, 1979 in Ratchaburi, Thailand. She got a Bachelor's Degree of Science in Chemistry from Chulalongkorn University in 2001. Since then, Miss Pattaraporn Pangnakorn has been a graduate student in Organic Chemistry division at department of chemistry, Chulalongkorn University. During the Master's Degree, Miss Pattaraporn Pangnakorn was awarded a teaching assistant scholarship by the Faculty of Science during 2003-2004 and was also awarded supported by a research grant from the Graduate School, Chulalongkorn University.

Miss Pattaraporn Pangnakorn's address is 197 Salacheep15 Salacheep Road Prachuabkhirikhun 77000, Tel. 032-611620, 0-6324-3898.



สถาบันวิทยบริการ
จุฬาลงกรณ์มหาวิทยาลัย